IOP Publishing Reports on Progress in Physics
Rep. Prog. Phys. **77** (2014) 093902 (20pp) doi:10.1088/0034-4885/77/9/093902

Report on Progress

Magnetic field modulated microwave spectroscopy across phase transitions and the search for new superconductors

Juan Gabriel Ramírez[1], Ali C Basaran[1], J de la Venta, Juan Pereiro and Ivan K Schuller

Department of Physics and Center for Advanced Nanoscience, University of California San Diego, La Jolla, CA 92093, USA

Received 16 January 2014, revised 16 April 2014
Accepted for publication 3 June 2014
Published 15 September 2014

Invited by Laura Greene

Abstract

This article introduces magnetic field modulated microwave spectroscopy (MFMMS) as a unique and high-sensitivity technique for use in the search for new superconductors. MFMMS measures reflected microwave power as a function of temperature. The modulation induced by the external ac magnetic field enables the use of phase locked detection with the consequent sensitivity enhancement. The MFMMS signal across several prototypical structural, magnetic, and electronic transitions is investigated. A literature review on microwave absorption across superconducting transitions is included. We show that MFMMS can be used to detect superconducting transitions selectively with very high sensitivity.

Keywords: superconductivity, microwave absorption, magnetic phase transitions, MFMMS

(Some figures may appear in colour only in the online journal)

1. Introduction

One of the most fundamental discoveries in condensed matter physics in the last century was the appearance of the superconducting state of matter [1]. Superconducting materials exhibit zero electrical resistance and expel the magnetic field (Meissner effect), when cooled down below a critical temperature (T_c). The physical origin of the transition from the normal to the superconducting state is only partially understood. Conventional superconductivity, which applies mainly to low temperature superconductors, can be described microscopically by Bardeen-Cooper-Schrieffer (BCS) theory [2]. However, the mechanisms behind high temperature superconductivity [3] and the new emerging Fe-based superconductors [4, 5] are still under debate.

Synthesizing novel superconductors has been an ongoing challenge in the field since their discovery. As of today, there is no fully accepted theory that can describe and predict the superconductivity in a given material system from basic physical quantities, such as crystallographic and electronic structure. Therefore, most of the new superconductors have been discovered through Edisonian-type searches, using the intuition of experimental scientists. In order to increase the chances of finding new superconducting materials, a combinatorial search can be used [6]. This method is based on the synthesis of inhomogeneous samples consisting of several phases with different stoichiometries. The use of a technique that can detect superconductivity selectively and with very high sensitivity would enable probing of all present phases in a sample at the same time. Superconducting quantum interference device (SQUID) magnetometers typically can detect a few micrograms of superconducting materials; however, they are also sensitive to all types of magnetic responses as well as contributions from the sample environment. This can lead to data misinterpretation and minor superconducting signals can be

[1] These authors contributed equally to this manuscript.

missed. Electrical transport measurements can only be done in continuous samples since percolation of the supercurrent is needed in order to obtain zero resistance. These kinds of difficulties can be overcome with an alternative technique; magnetic field modulated microwave spectroscopy (MFMMS) which is based on the measurement of the field derivative of the microwave absorption as a function of temperature.

Microwave absorption of a material drastically changes when the material crosses a superconducting transition. This has been measured on an extensive number of superconductors in different forms (powders [7–16] and single crystals [17–21]). However, a change in the microwave absorption associated with other types of transitions could also be possible. Since the search for 'new superconducting materials' involves a very broad range of temperature scans, the ability to distinguish the superconducting from non-superconducting transitions is crucial. This especially comes into prominence when an 'unknown' material is investigated. In this review we introduce MFMMS as a powerful technique in the search for new superconductors. We highlight the main advantages of MFMMS in terms of its sensitivity and selectivity when combining with low field scans.

We first introduce a brief theoretical background of microwave absorption in normal metals and superconductors. In section 3, we review several experimental studies on superconductivity by microwave absorption techniques. We focus on the differences between three techniques: cavity perturbation, direct absorption, and field-modulated absorption. Section 4 is dedicated to the MFMMS setup, and its signal interpretation. We show the MFMMS signal intensity dependence on microwave power, dc magnetic field, and modulation field following a demonstration of the sensitivity of the technique. Section 5 shows the MFMMS signal across different types of superconducting and non-superconducting phase transitions. We discuss the selectivity of the MFMMS technique in section 6. A possible route for searching for new superconducting materials in combination with the MFMMS technique will be given in section 7. Finally, we present our conclusions and an outlook.

2. Microwave absorption: theory

In this section, we briefly describe the physical processes behind microwave absorption in metals and superconductors. We include some examples that illustrate the dependence of the absorption mechanism across superconducting transitions.

2.1. Normal metals

The conductivity of a metal is defined as $\tilde{\sigma} = \sigma_1 + i\sigma_2$ when an oscillating electric field with a frequency ω_{mw} is applied. Here, σ_1 and σ_2 account for the carriers that can and cannot move in phase with the applied field, respectively [13].

The surface impedance (Z_s) represents the ratio between the electric and magnetic field components along the surface of the material ($\epsilon_{\parallel,mw}$ and $h_{\parallel,mw}$, respectively) and can be written as

$$Z_s \equiv \frac{\epsilon_{\parallel,mw}}{h_{\parallel,mw}} = \sqrt{\frac{i\mu_0\omega_{mw}}{\sigma_1 - i\sigma_2}} = R_s + iX_s, \tag{1}$$

where R_s and X_s are the surface resistance and reactance, respectively. ω_{mw} is the microwave frequency and μ_0 is the magnetic permeability of vacuum.

Due to the high density of free carriers, metals tend to shield most of their volume from electromagnetic radiation. The electromagnetic waves extend into a conductor with a characteristic distance. This length is defined as the skin depth (δ) for metals and penetration depth (λ) for superconductors. In metals, the local limit is reached when the mean-free-path of the carriers is smaller than δ. At microwave frequencies, the local limit implies $\sigma_1 \gg \sigma_2$. In this limit the R_s and X_s are equal for normal metals and can be expressed as

$$R_s(T, \omega_{mw}) = X_s(T, \omega_{mw}) = \sqrt{\frac{\mu_0\omega_{mw}}{2\sigma_1}}. \tag{2}$$

The penetration depth of microwaves is defined for non-magnetic metals [17],

$$\delta = \sqrt{\frac{2}{\mu_0\omega_{mw}\sigma_1}}, \tag{3}$$

and can be generalized to magnetic metals as

$$\delta_m = \sqrt{\frac{1}{\mu(h,T)\omega_{mw}\sigma(h,T)}}, \tag{4}$$

where $\sigma(h, T)$ is the field and temperature dependent complex conductivity and $\mu(h, T)$ is the magnetic permeability of the material [17, 22].

In general, the absorbed electromagnetic power (P) can be expressed in terms of the surface resistance as

$$P = \frac{1}{2}\int\int R_s(T,\omega)\, h_{mw}^2\, dA, \tag{5}$$

where dA is a differential area perpendicular to the surface of the material and h_{mw} is the magnetic field component of the electromagnetic wave.

2.2. Superconductors

In the case of superconductors, there are three main dissipation mechanisms: dissipation due to the non-superconducting electrons, pair braking due to transitions across the superconducting band gap (Δ), and vortex motion. Therefore, the surface resistance and reactance of a superconducting material is expected to be affected by all these three mechanisms. The contribution from each of these mechanisms will be discussed further in the manuscript. At high temperatures and very low fields the most important contribution comes from the non-superconducting electrons since the microwave frequency has an energy smaller than the gap and at low fields little or no flux motion is expected. The surface resistance and reactance of superconductors due to the non-superconducting electrons can be approximated in the local limit ($\lambda \gg \xi$ where ξ is the coherence length) in which $\sigma_2 \gg \sigma_1$, and thus R_s and X_s are given by [17]

$$R_s = \frac{1}{2}\mu_0^2\omega_{mw}^2\lambda^3\sigma_1,$$
$$X_s = \mu_0\omega_{mw}\lambda. \tag{6}$$

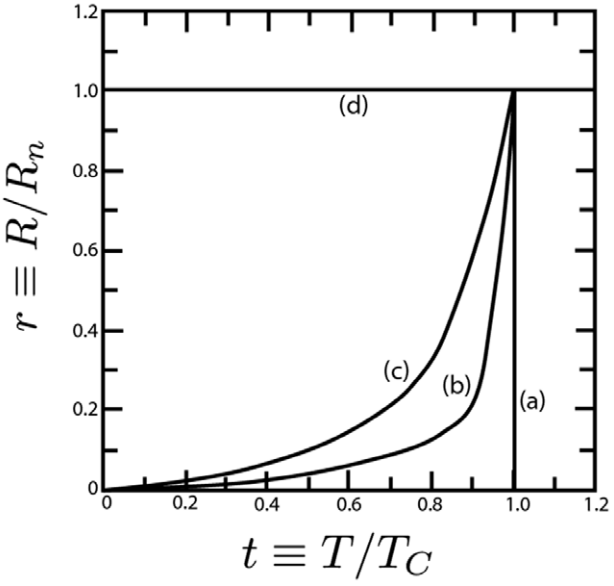

Figure 1. Sketch of the surface resistance ratio (R/R_n) as a function of reduced temperature (T/T_c) for several frequencies ranging from dc (curve (a)) to infrared (curve (d)) for a superconducting transition. Reprinted with permission from [11]. Copyright 1958 by the American Physical Society.

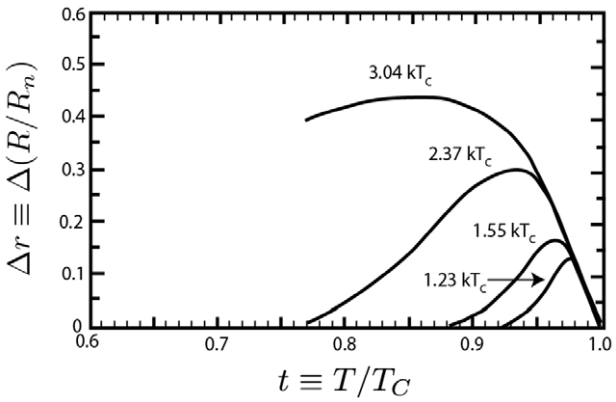

Figure 2. Excess microwave absorption in aluminum ($T_c = 1.175$ K) due to transitions across the gap for different frequencies expressed in terms of kT_c ($kT_c \sim 24.475$ GHz). Adapted with permission from [23]. Copyright 1957 by the American Physical Society.

The decrease of surface resistance for superconductors was first measured by London [23], and then by Pippard, a few years later [24, 25]. Figure 1 shows the surface resistance ratio, $r \equiv R/R_n$, (where R and R_n refers to surface resistance below and just above the superconducting transition, respectively) as a function of reduced temperature across the transition. The surface resistance has a maximum decrease at zero-frequency (figure 1, line (a)), while there is almost no change at infrared frequencies (figure 1, line (d)). This frequency-dependent behavior was interpreted as an indication of the existence of a superconducting gap [11] and confirmed across the superconducting transition of aluminum [23]. In figure 2, microwave absorption due to the dissipation from non-superconducting electrons (equation (6)) has been subtracted from the total microwave absorption in order to illustrate the

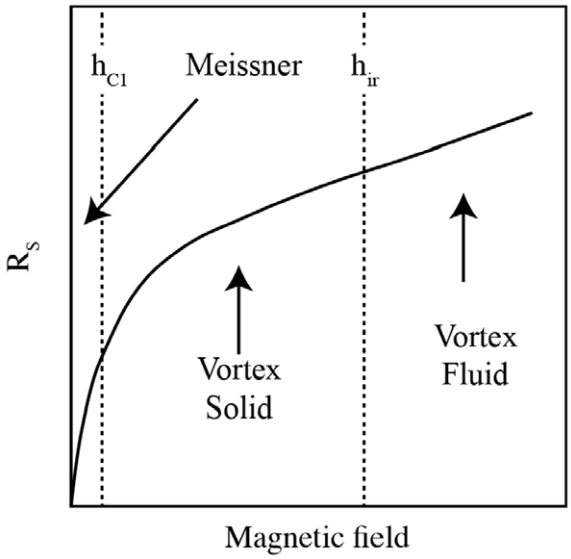

Figure 3. Simplified sketch of the surface resistance (R_s) of a type II superconductor as a function of the external magnetic field. Reprinted from [17] with kind permission from Springer Science and Business Media. Copyright 1999 Springer.

contribution of pair breaking effects. The response for different wavelengths ranging from 30.10 to 74.40 GHz indicates the frequency dependence. Pair breaking effects are negligible at temperatures below the onset of r [9, 23]. The estimated value of the superconducting band gap as a function of temperature agrees with BCS theory.

In type II superconductors, the existence of vortices and vortex movement contributes as an additional source for dissipation of electromagnetic energy. Depending on the magnetic field, temperature, and pinning strength, it is possible to identify three different regions (figure 3, [17]): Below the first critical field (h_{c1}) the material is in the Meissner state and the surface resistance can be described by equation (6). Within this region, the absorption increases with the applied field and can be expressed as a function of λ. At fields higher than h_{c1}, the magnetic flux lines penetrate into the superconductor and vortices are created. The irreversibility field (h_{ir}) determines when the vortices unpin and start moving. Above h_{ir}, the absorption loses its initial nonlinear increase becoming linear in the vortex fluid region.

The effects of vortex pinning and flux creep on the surface impedance of a material as a function of the frequency, dc field and temperature are described in [24]. Figure 4 shows the surface resistance as a function of reduced temperature at a frequency of 10 GHz for (a) no applied field, (b) applied field above h_{c1} but below the irreversibility field and (c) at a high enough field to create flux creep, including thermally activated flux flow. This shows that vortices produce an increase in the surface resistance, even if vortex movement is not present.

3. Microwave absorption: experiments

In microwave absorption experiments the instrumental setup defines the physical parameters that can be studied. For example, cavity resonators allow higher sensitivity and better

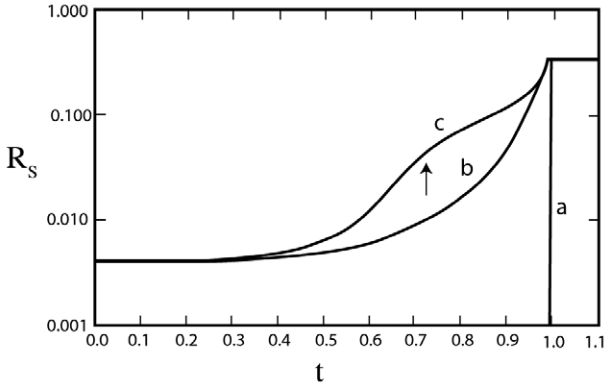

Figure 4. Calculated surface resistance (in ohms) as a function of the reduced temperature ($t \equiv T/T_c$) at 10 GHz (*a*) $h_{dc} = 0$, (*b*) $h_{c1} < h_{dc} < h_{ir}$ and (*c*) vortices with flux creep and thermally activated flux flow included. Please note that the logarithmic scale is in R_s. Reprinted with permission from [24]. Copyright 1991 by the American Physical Society.

control of the electromagnetic field distribution, while coplanar waveguides allow continuous change of the frequency. In this review, we consider the microwave absorption experiments performed in cavity resonators.

Depending on the amount of output power required, either vacuum tube systems (i.e. klystron) or solid-state devices (i.e. Gunn diodes) are used as microwave sources. The microwave source is connected to the cavity through a waveguide. A Schottky diode (silicon or gallium arsenide) is used to detect the reflected microwaves. The microwave power can typically be varied from 0.01 to 200 mW using a variable attenuator.

The instruments can be designed to record either the relative change of the resonance frequency and quality factor ($\Delta f/f_0$ and $\Delta Q/Q_0$) with respect to the empty cavity or just the reflected intensity.

3.1. General cavity setup

When a sample is placed inside a microwave cavity resonator, it is exposed to a standing electromagnetic wave. If the sample is small enough, the field distribution can be considered uniform. A cavity resonator can be described by its quality factor (Q), which is inversely proportional to the energy dissipated within the cavity. Typical cavities which have quality factors of around 10^4 are made of oxygen-free copper. In order to increase the sensitivity of the measurements, superconducting (Nb coated) cavities or shielded dielectric resonators (sapphire, TiO_2) are commonly used [25, 26]. These setups do not allow frequency-dependent measurements since cavities resonate at specific frequencies.

We classify cavity-based techniques according to the physical parameters measured: resonance frequency and quality factor (section 3.1.1), direct microwave absorption (section 3.1.2) and field derivative of the microwave absorption (section 3.1.3). Figure 5 sketches the signal as a function of temperature when a superconducting sample is measured across T_c at frequencies $\hbar\omega \ll \Delta$.

3.1.1. Cavity perturbation method. The cavity perturbation method correlates the changes in the quality factor Q and resonance frequency f (relative to the empty cavity, Q_0 and f_0) to the surface impedance under certain approximations. It requires deconvoluting the effects arising from the cavity and temperature fluctuations and measuring changes between $R_n \sim 10^{-5}$ to 10^{-9} ohms [27]. The resonators used in these setups are made of dielectric materials (such as sapphire [25, 28] or TiO_2 [26]) coated with oxygen-free copper or superconductors. Their characteristic quality factors are on the order of $\sim 10^6$ [29–31].

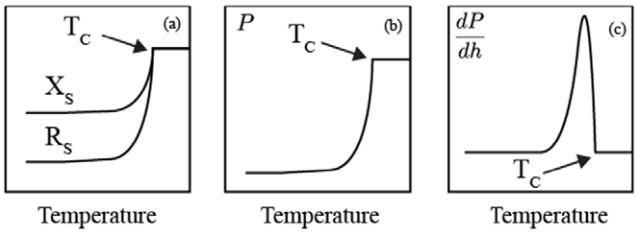

Figure 5. Sketch of the measured signal as a function of temperature across the superconducting transition at frequencies ($\hbar\omega_{mw}$) lower than the superconducting gap energy (Δ). Each image represents a different experimental method: (*a*) Surface resistance, R_s, and surface inductance, X_s, obtained from cavity perturbation methods, (*b*) measurement of the direct absorption, P, and (*c*) field-derivative of the absorbed power.

This method has been used to obtain the ac conductivity at microwave frequencies. Surface impedance measurements as a function of temperature contain information on the electronic structure of quasiparticles and they can provide evidence for characteristics related to unconventional superconductivity such as gap nodes, strong anisotropy, and multiband-energy gaps [32, 33]. Other studies reviewed the theory [34], experimental setups [35] and applications [36]. A generalization that accounts for different electromagnetic modes and sample geometries was also reported [37]. The results of the study of high temperature superconductors by cavity perturbation method was summarized in [13].

3.1.2. Direct microwave power absorption. The setups for direct microwave power absorption are similar to electron paramagnetic resonance (EPR) spectrometers with typical frequencies between 10 and 35 GHz. After the discovery of high T_c superconductors, these measurements were used to probe the vortex state using a rather modest external magnetic field ($\sim$10 Oe) [14]. A typical curve of type II superconductors in the direct power absorption mode is depicted in figure 5(*b*) where a rapid reduction of the signal at the transition is shown. A correlation of the microwave absorption with the grain size of the powders was found, and a similar relationship was measured by magnetic susceptibility [10, 12, 14, 15, 38]. A different approach for direct microwave power absorption has been shown using a reference EPR signal [39].

3.1.3. Field-derivative of the microwave power absorption. This technique is similar to the direct microwave absorption, but during the measurement a modulated external magnetic field is applied. The modulation field has a typical frequency of 100 KHz and amplitude ranging from 0.1 to 50 Oe. The

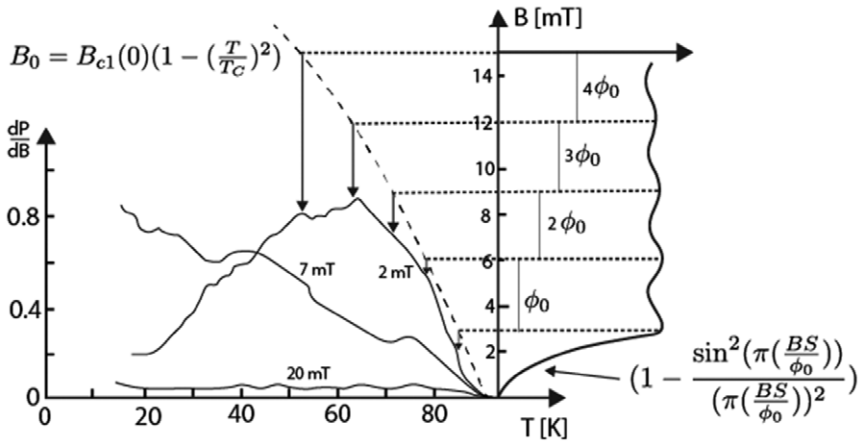

Figure 6. Correspondence between the local maxima of the field-modulated microwave absorption and the successive flux penetration as a function of temperature for a granular $YBa_2Cu_3O_{7-d}$ ceramic sample. ϕ_0 corresponds to quantum flux, S is the effective surface area of the Josephson loops and B represents the external magnetic field. $B_{c1}(0) = 23$ mT is used. Reprinted from [40] with kind permission from Springer Science and Business Media. Copyright 1991 Springer.

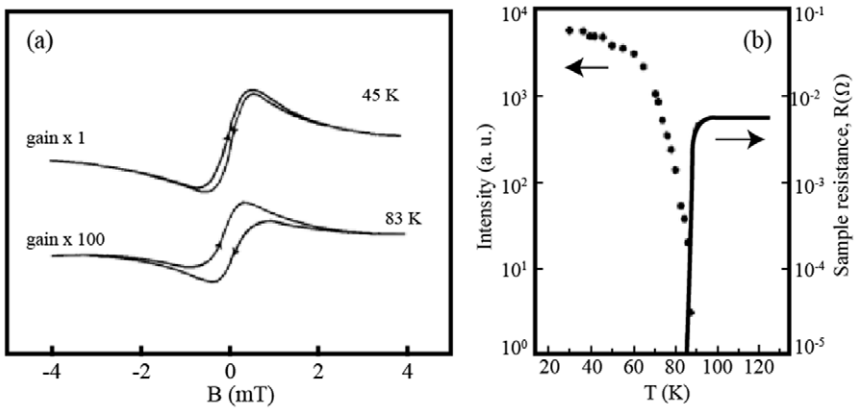

Figure 7. (*a*) Field-derivative of the microwave absorption as a function of the magnetic field for two different temperatures below T_c on a $GdBa_2Cu_3O_{9-y}$ sample. (*b*) Signal intensity (peak-to-peak) at different temperatures (left axis) and dc resistance (right axis). Reprinted with permission from [45]. Copyright 1987 IOP Publishing Ltd.

modulated output signal increases the sensitivity and enables phase sensitive detection.

Field-modulated microwave absorption data can be acquired as a function of the external magnetic field or temperature. These two methods give complementary information about the dissipation processes. A relationship between these two measurements was shown in the case of granular $YBa_2Cu_3O_{7-d}$ samples [40] (see figure 6). In this case the temperature sweep presents a series of maxima, which correspond to fluxons entering the superconducting material and causing an oscillation of the absorbed power.

3.1.3.1. Field sweep. A significant nonlinear hysteresis can be observed in the field sweep mode [41–43]. The modulation of the vortex density in the superconducting state explains the overall behavior of the signal while the modulation of their depinning is responsible for the hysteresis [43, 44].

Magnetic field modulated setup was used to measure the microwave absorption as a function of the external field at various temperatures for $GdBa_2Cu_3O_{9-y}$ (figure 7(*a*)). A hysteretic behavior is observed when the external magnetic field is swept. Figure 7(*b*) shows the signal intensity variation as a function of temperature. The interpolation of the intensity to zero is close to the critical temperature determined by transport measurements.

The non-resonant absorption measurements at low magnetic field were mostly devoted to the understanding of the hysteresis mechanism and the role of the granularity of the new high temperature superconductors [41,46–49]. The main loss mechanisms are usually explained in terms of weakly coupled superconducting domains, i.e. grains in ceramics and twins in single crystals [50–52]. Magnetic fields far below the critical field penetrate across the weak links and give rise to microwave absorption [53]. This method is currently used to study the intergranular and intragranular pinning effects [54, 55].

3.1.3.2. Temperature sweep The measurement of the field derivative of the microwave absorption as a function of temperature can be found in the literature under several names [40, 56, 57]. However, most of these techniques just differ in minor details, i.e. magnetically modulated microwave

Table 1. Compilation of references where the modulated microwave absorption on temperature sweep mode has been employed to find superconducting materials.

Material	Form	References
$YBa_2Cu_3O_{7-x}$	Single crystal	[60,78–83]
$\kappa-(ET-d_s)_2Cu(NCS)_2$	Crystal	[84–86]
$\kappa-(ET)_2Cu[N(CN)_2]Br$	Crystal	[84–86]
$\kappa-(BED-TTF)_2\,Cu(NCS)_2$	Crystal	[68]
$Sm_{2-x}Ce_xCuO_{4-\delta}$	Single crystal	[87]
$Pr_xGd_{1-x}Ba_2Cu_3O_7$	Thin films	[61]
$PbBi_2Sr_2Ca_2Cu_3O_y$	Powders	[8]
$Y_xNiB_{1-x}C_y$	Thin films	[62]
K_xC_{60}	Films and bulk	[77]
$Tl_2Ba_2CaCu_2O_8$	Single crystal	[88]
$Bi_2Sr_2CaCu_2O_8$	Single crystal	[88]
La_2C_3 and La-β	Powders	[6]

absorption (MMMA) and MFMMS can be considered the same technique.

The temperature dependence of the field-modulated absorption can be measured in terms of either transmitted [58] or reflected powers [10, 12, 30, 59]. Here, we mainly consider measurements of the reflected microwave power while the sample is subject to a modulation field [59]. This produces a peak-like signal across a superconducting transition (figure 5(*c*)), allowing for an unambiguous detection of superconducting phases [59–62]. Although the exact quantitative interpretation of the signal is still under investigation, these measurements can be used to identify minute superconducting phases in a fast, sensitive and reliable way.

The signal can be understood in a more intuitive way if we consider that, close to the transition temperature, the modulated field drives the material in and out of the superconducting state and produces a strong increase of the absorption signal. Figure 8 shows the relationship between the field and temperature sweep in a superconductor [59, 63].

Modulated microwave absorption on temperature sweep mode has been used to measure twin boundaries in high-T_c superconductors [49, 64], $Bi_2Sr_2CaCu_2O$ whiskers [65], powder and bulk MgB_2 [66, 67], organic superconductors [68], and more recently, ternary borides Mo_2Re_3B and Mo_3Re_2B [69]. Correlation of the MFMMS signal with the dc magnetization [70] and comparison with the direct absorption technique (no modulation) was addressed for $YBa_2Cu_3O_{7-x}$ [71, 72]. Similar approaches have been used in other systems like $PbBi_2Sr_2Ca_2Cu_3O_y$ [8]. More recently strong vortex pinning was found in $SmO_{1-x}F_xFeAs$ [55]. Studies on the MFMMS signal noise and corrections to the measured critical fields of $YBa_2Cu_3O_{7-x}$ can be found in [73, 74]. Type I superconductors were also studied by this technique, i.e. lead [75], mercury [76], tin and indium [53]. Comparison of type I and high T_c superconductors implies that the main absorption mechanisms in high T_c superconductors are due to vortex motion and the nucleation of vortices at the surface of the material [53].

Several superconductors have been discovered using microwave absorption techniques, i.e. potassium-doped fullerenes with a T_c of 18 K [77]. The combination of phase spread alloy growth methods and MMMA was proposed to search for new superconducting materials [61]. Using this approach superconductivity was found in La_2C_{3-x} [6]. The relationship between the superconducting transition temperature of $Pr_xGd_{1-x}BaCu_3O_7$ estimated from microwave and dc transport measurements is shown in figure 9 [62]. Table 1 lists some of the works that have employed this technique in the search for new superconductors.

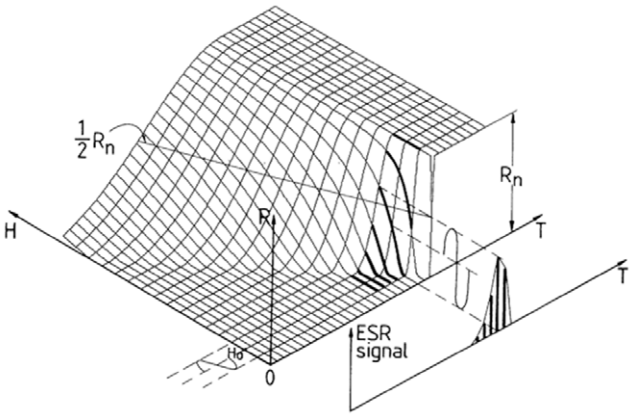

Figure 8. Magnetically modulated microwave spectroscopy as a consequence of the field derivative of the surface resistance R_s (R on the graph). The electron spin resonance (ESR) signal, labeled 'ESR signal' in the original report, produces a peak when R_s changes as a function of field in a way similar to the dc resistance. The signal is composed of several $R_s(T)$ curves for different fields across h_{c2}. Reprinted with permission from [63]. Copyright 1991 by the American Physical Society.

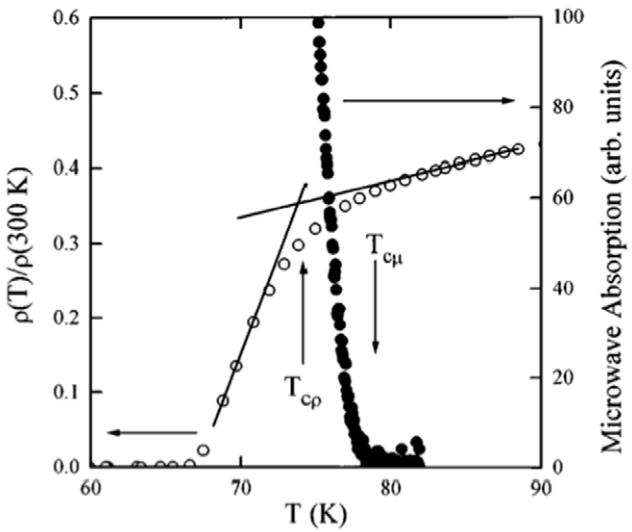

Figure 9. Normalized resistivity and field-modulated microwave absorption signal as a function of temperature for a $Pr_xGd_{1-x}BaCu_3O_7$ film with 5% Pr. The superconductivity onset temperatures corresponding to the two techniques are indicated. Reprinted with permission from [61]. Copyright 1995 AIP Publishing LLC.

3.1.4. Other remarks. The measurement of MFMMS across non-superconducting phase transitions is scarce. MMA measurements were used to compare different types of superconductors to magnetic materials [89]. It was observed

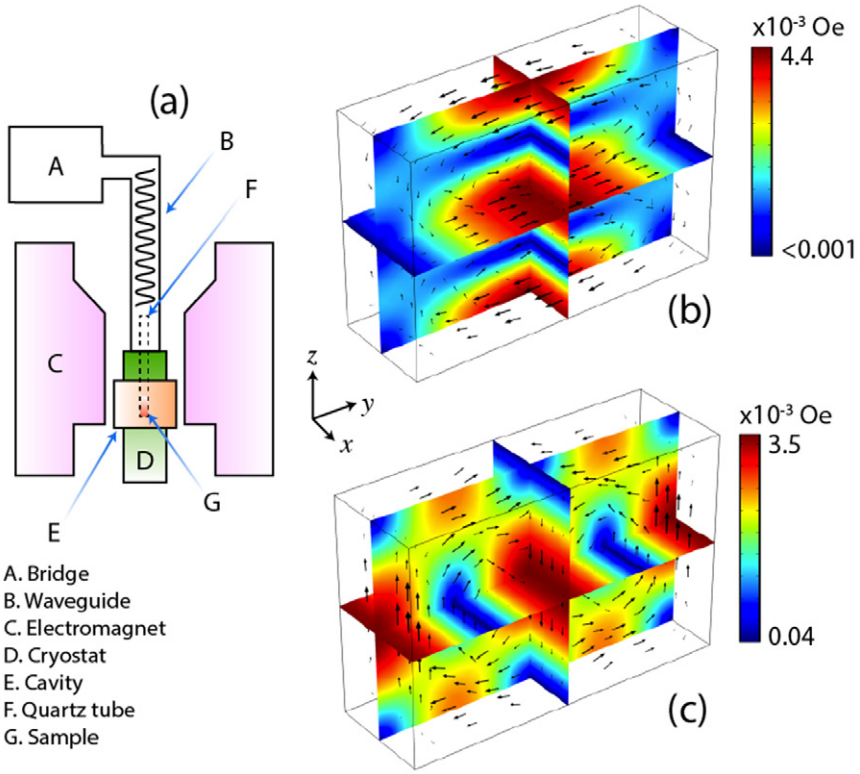

Figure 10. (*a*) Sketch of the MFMMS setup. (*b*) and (*c*) represent density plots of the magnetic field distribution inside the cavity resonator. Red and blue colors correspond to maximum and minimum intensities, respectively. Black arrows depict the magnetic field direction in a single period of the microwave signal. By changing from 9.6 GHz (*b*) to 9.4 GHz mode (*c*), the magnetic field component of the electromagnetic wave can be adjusted to be parallel or perpendicular to the external field. The values of the resonance frequencies refer to an empty cavity at room temperature with a constant flow of nitrogen. Plots were obtained by finite element analysis using COMSOL Multiphysics.

that the superconductors and materials exhibiting a strong change in the magnetoresistance [90] produce a similar derivative signal when the magnetic field is swept. However, it was shown that the hysteresis of the low-field absorption signal can be used to differentiate superconducting transitions from magnetic transitions [91–93]. A comprehensive comparison of temperature sweep signals for various types of phase transitions has not been reported.

In the following sections, we address the field derivative microwave absorption signal in the temperature sweep mode in more detail. The influence of the experimental parameters (external field, modulation field and microwave power) on microwave signal will be shown using known superconducting materials. Further details of the techniques described above can be found in [94] and references therein.

4. MFMMS technique and setup

4.1. Setup

MFMMS uses a customized X-band EPR apparatus. It includes a microwave circuit, a phase sensitive detector, an electromagnet, a cavity resonator, and a flow cryostat. The cryostat allows sweeping of the sample temperature between 3.8 and 300 K (see figure 10(*a*)). The dual-mode cavity can be used to produce two resonances at 9.4 and 9.6 GHz that correspond to modes where the magnetic field is perpendicular (TE_{012} mode, figure 10(*c*)) or parallel (TE_{102} mode, figure 10(*b*)) to $\hat{z}$, respectively. An automatic frequency controller (AFC) continuously adjusts the microwave frequency to the resonance frequency of the cavity. The sample is placed at the center of the cavity where ε_{mw} is minimum and h_{mw} is maximum. In addition to h_{mw}, the sample is exposed to an external dc (h_{dc}), and an ac (h_{ac}) magnetic field. The microwave field is used to probe the sample as the temperature is swept; $h_{dc} + h_{ac}$ are used to enhance the absorption, reduce the background noise and increase the sensitivity. h_{ac} produces a modulation of the reflected power P at a frequency of ω_{ac}.

4.2. MFMMS signal

System calibration was performed using superconducting Nb thin films grown on sapphire either by molecular beam epitaxy (MBE) or rf sputtering. MBE films were grown in a system with base pressure of 10^{-10} Torr. The sample thickness obtained by x-ray reflectometry was 150 nm. Rf-sputtered samples were grown from a Nb target in a vacuum chamber with a base pressure of 10^{-7} Torr. The deposition was performed at 4 mTorr Ar and 100 W rf power. The thickness of sputtered samples was 100 nm. Sapphire substrates were chosen because of their low microwave absorption and high thermal conductivity. In our standard configuration, the size of the samples can be up to 3×4 mm^2 area.

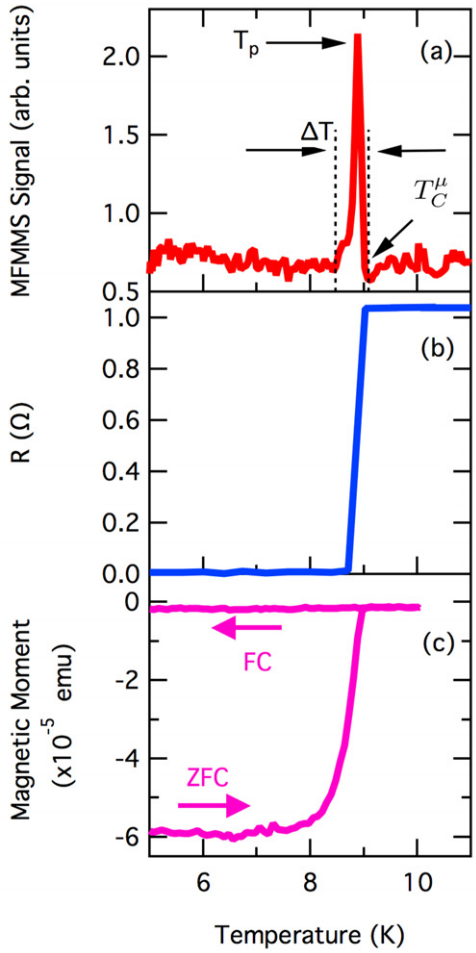

Figure 11. (*a*) MFMMS signal as a function of temperature for a Nb thin film with an applied dc magnetic field of 500 Oe parallel to the surface of the sample. The peak temperature T_p, transition temperature T_c and transition width ΔT are shown. The temperature is swept from 11 to 5 K. The resistance (*b*) and magnetic measurements (*c*) are shown as a function of temperature for the same sample at the same magnetic field. Arrows in (*c*) indicate the temperature sweep direction (ZFC and FC respectively). The sample dimensions are 150 nm thick and 2×2 mm^2 surface area (6×10^{-7} cm^3) of Nb.

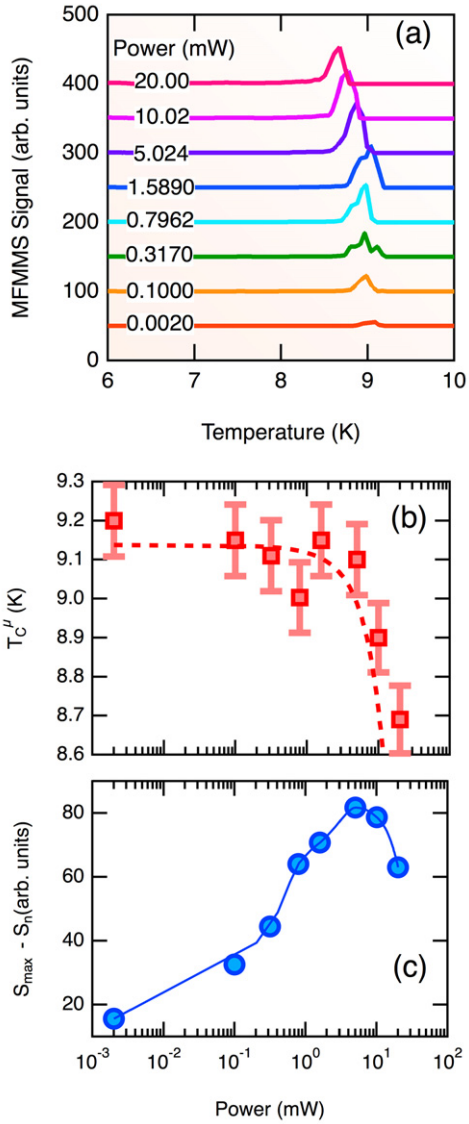

Figure 12. (*a*) MFMMS signal as a function of temperature obtained for different applied microwave powers for 150 nm thick Nb film. The curves are shifted vertically for clarity. (*b*) Transition temperature (T_c^μ) and (*c*) maximum absorption ($S_{max} - S_n$) extracted from MFMMS curves as a function of applied microwave power.

MFMMS results for superconducting Nb films are shown in figure 11(*a*). For comparison, we also include a standard four-probe resistance (figure 11(*b*)) and zero field cooled (ZFC) and field cooled (FC) SQUID magnetometry measurements for the same sample (figure 11(*c*)). In all cases a 500 Oe magnetic field was applied parallel to the sample surface. MFMMS measurements were done using the dual-mode cavity with the microwave magnetic field parallel to the modulation and external dc magnetic fields. The temperature was swept from 11 to 5 K at a constant rate of 3 K min^{-1}. The superconducting transition temperature ($T_c^\mu = 9.1$ K) obtained from MFMMS coincides with the other two measurement techniques. The transition width from the MFMMS measurement (ΔT) was 0.5 K.

Although the exact shape, symmetry, and amplitudes can vary, the superconducting transition produces a peak-like MFMMS signal. The transition temperature determined by the MFMMS measurement (T_c^μ) is the onset of the drastic change. The main characteristics of the signal for small dc fields can be seen as follows. The signal is in the noise floor for temperatures above T_c and increases abruptly at the T_c. The signal reaches a maximum at a certain temperature (T_p) and decreases back to the noise level measured above T_c. Other important parameters are the full width at half maximum of the peak (ΔT) and the maximum MFMMS signal intensity (S_{max}) with respect to the MFMMS signal in the normal state (S_n), i.e. just above T_c.

4.2.1. Microwave power dependence. The dependence of the MFMMS signal on applied microwave power is shown in figure 12(*a*) for the same 150 nm thick Nb film. The external magnetic field was 15 Oe. If there is no background, the MFMMS signal in normal state is independent of the applied microwave power. Increasing the microwave power

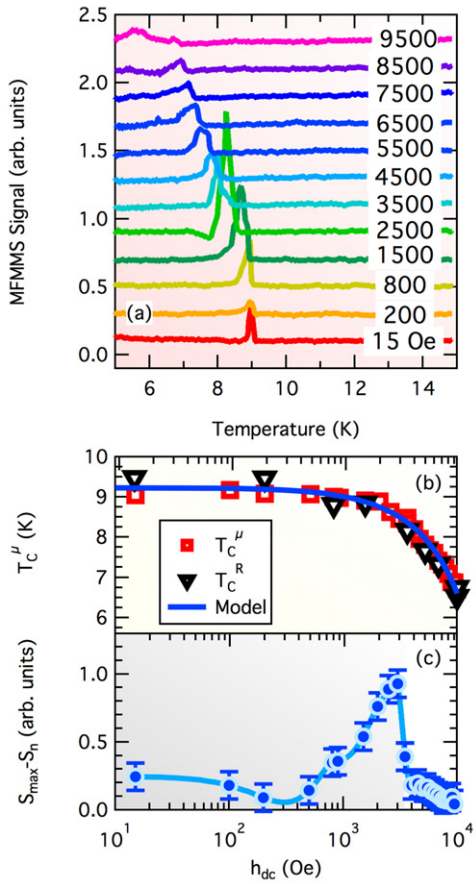

Figure 13. (*a*) MFMMS signal as a function of temperature for a 150 nm Nb Film at various dc applied magnetic fields, h_{dc}. (*b*) Transition temperature T_c^μ extracted from (*a*) (open squares) compared to the transition temperature extracted from resistance measurements (inverted open triangle). The line corresponds to a non-linear fit of the T_c^μ values of equation (7) (see text), which gives $T_c = 9.22$ K and $h_{c2} = 1.7$ kOe. (*c*) $S_{max} - S_n$ as a function of the magnetic field.

suppresses the transition to lower temperatures (figure 12(*b*)) while increasing the peak intensity ($S_{max} - S_n$, figure 12(*c*)). The decrease in T_c^μ is attributed to heating of the sample produced by the microwave power. The transition temperature changes from 9.2 to 8.7 K as the microwave power varies from 0.002 to 20 mW.

Another superconducting system, $ErRh_4B_4$, was measured to check the microwave power dependence (not shown) in metallic bulk samples rather than thin films. No changes in T_c^μ as a function of microwave power up to 20 mW were detected. This might be related to the fact that microwaves only affect the surface of the bulk samples and induced heat can be neglected. In order to maximize the signal to noise ratio (SNR), we employed 1 mW as a standard microwave power in all measurements (unless otherwise specified).

4.2.2. DC magnetic field dependence. Selected MFMMS curves measured in dc magnetic fields between 15 Oe and 9.5 kOe are shown in figure 13(*a*). The superconducting transition temperature decreases from 9.2 to 6 K with increasing magnetic field (h_{dc}) as shown in figure 13(*b*) (open squares). Note the logarithmic scale in the horizontal axis. For applied fields below 500 Oe there is no significant change in the transition temperature. Above 500 Oe, T_c^μ decreases and reaches 6 K at 9.5 kOe in good agreement with T_c^R obtained from resistance measurements (inverted triangles on figure 13(*b*)). The field dependence of the critical temperature is given by

$$T_c\,(h_{dc}) = T_c^0\sqrt{1 - \frac{h_{dc}}{h_{c2}}}, \tag{7}$$

where T_c^0 corresponds to the transition temperature at zero magnetic field. Figure 13(*b*) shows a fit to equation (7) as indicated by the solid line. The critical temperature and magnetic field values are obtained as 9.2 K and 1.7 T, respectively. The results obtained from MFMMS are in good agreement with resistance and SQUID measurements and follow the expected behavior [95].

The maximum MFMMS signal intensity relative to the normal state ($S_{max} - S_n$) as a function of the applied magnetic field is shown in figure 13(*c*). The signal remains constant up to 200 Oe, followed by an increase for fields up to 3 kOe. At higher fields, $S_{max} - S_n$ decreases, reaching values close to the background level at 9.5 kOe. It is important to mention that for fields larger than 8 kOe, the MFMMS signal shows a wider peak, which complicates the estimate of T_c^μ. The behavior of $S_{max} - S_n$ as a function of dc magnetic field varies from system to system. In order to make sure the superconductor is not suppressed by the external magnetic field, we only apply a very small field (15 Oe) when investigating potentially new superconducting materials.

4.2.3. Modulation field dependence. The dependence of the the MFMMS signal with the modulation field was investigated using 15 Oe external field and 1 mW microwave power. The same 150 nm thick Nb sample was measured by varying h_{ac} between 5 and 15 Oe. As a result, the total applied field ($h_{dc} + h_{ac}$) was always positive to avoid field-dependent hysteretic effects [59]. The results are shown in figure 14(*a*) where the curves have been vertically shifted for clarity. The background level was the same for all the curves. T_c^μ is independent from the modulation field up to 15 Oe (figure 14(*b*)). Figure 14(*c*) shows that $S_{max} - S_n$ is proportional to h_{ac} as indicated by the linear fit. The peak width is also constant as a function of the modulation fields.

4.3. MFMMS sensitivity

In order to determine the sensitivity of the MFMMS technique, we used 100 nm thick Nb films patterned with standard lithographic techniques to vary the total superconducting volume. A set of test samples between 10^{-7} and 10^{-12} cm^3 of Nb were prepared using electron beam lithography. The samples were also compared to an unpatterned Nb film grown under the same conditions. In all measurements, the microwave power was kept at 1 mW and applied magnetic field at 15 Oe with 15 Oe modulation.

Figure 15(*a*) shows the MFMMS signal as a function of temperature for the continuous sample. The film shows a sharp

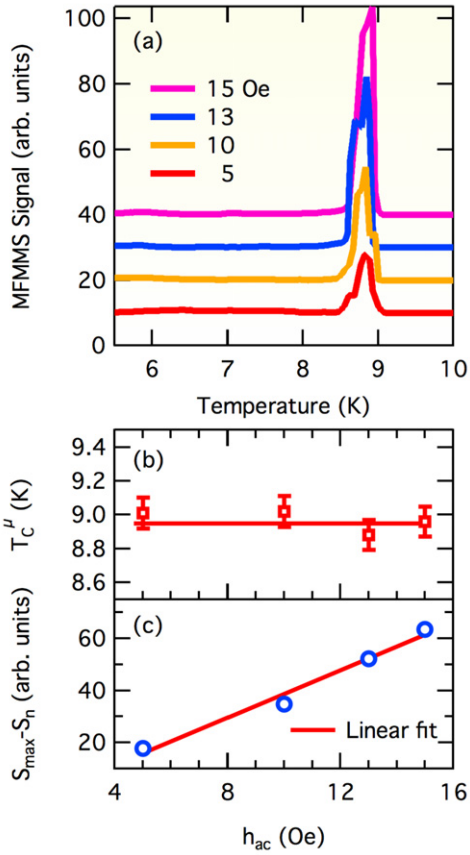

Figure 14. (*a*) MFMMS signal for a 150 nm Nb film at several modulation amplitudes, h_{ac}. (*b*) T_c^μ and (*c*) $S_{max} - S_n$ as a function of the modulation field parallel to the sample surface.

transition close to 7.75 K, with a maximum microwave signal at 7.5 K. The difference in sharpness of the peak compared to the MBE-grown Nb film (figure 11(*a*)) is related to the growth process, i.e. impurity level or crystallinity [59]. Figure 15(*b*) shows SQUID magnetometer measurements from the same sample. The critical temperatures determined by both methods are in good agreement.

Figure 15(*c*) shows the MFMMS signal for the patterned sample (100 nm × 10 μm × 10 μm), with a total volume of 10^{-11} cm^3 of Nb. Inset on figure 15(*c*) shows the optical image of patterned Nb. A clear superconducting transition peak appears well above the noise level. Considering the SNR (SNR = 10) of the MFMMS measurement, the obtained sensitivity is 10^{-12} cm^3. The T_c^μ extracted from the MFMMS data is around 6.8 K, significantly lower than that of the continuous film. The corresponding ZFC-FC measurements for the same sample show no evidence of superconductivity (figure 15(*d*)) due to the volume of superconducting material being within the sensitivity limit of SQUID magnetometers. However, the diamagnetic signal from the substrate is larger than the signal from Nb. This direct comparison highlights the advantage of MFMMS over SQUID magnetometry for the detection of a small amount of superconducting material in the presence of a paramagnetic/diamagnetic background signal.

5. Comparison of MFMMS signal across superconducting and non-superconducting phase transitions

We measured more than 200 samples undergoing several prototypical phase transitions to investigate the selectivity of MFMMS. This includes superconducting (elements, borocarbides, borides, pnictides, and cuprates) metal–insulator, paramagnetic–ferromagnetic, and paramagnetic–antiferromagnetic transitions. A short summary of the samples and their properties is presented in table 2. Measurements of non-superconducting phase transitions will be discussed in section 5.2.

5.1. MFMMS across superconducting transitions

In this section we show the MFMMS measurements of $ErRh_4B_4$ and MgB_2 as examples in order to demonstrate that the results obtained from Nb are applicable to other superconductors.

5.1.1. $ErRh_4B_4$. $ErRh_4B_4$ is an example of a reentrant superconductor [99]. The first superconducting transition occurs at 8.7 K followed by a ferromagnetic transition and reentrance to superconducting state at $T_{c2} = 0.9$ K. The ferromagnetic transition suppresses superconductivity due to reordering of Er local moments. The coexistence of the two phases around T_{c2} has been proven by neutrons [100–102], scanning tunneling microscope (STM) [102], and susceptibility measurements [101]. Surface impedance measurements of single crystal $ErRh_4B_4$ show anomalous effects close to T_{c2} due to spin fluctuations [103] and in general, similar anomalies are present in magnetic superconductors [104, 105].

MFMMS signal of an $ErRh_4B_4$ single crystal with 15 Oe applied field is shown in figure 16(*a*) with $T_c^\mu = 7.7$ K. The general shape of MFMMS signals is similar to sputtered Nb films. The behavior of T_c^μ as a function of different applied magnetic fields is plotted in figure 16(*b*). The transition temperature decreases with increasing applied field. The solid line corresponds to a fit to equation (7). The T_c (7.82 K) and h_{c2} (8.6 kOe) extracted from the fit are in agreement with earlier reports [106–108]. Figure 16(*c*) depicts the maximum MFMMS signal relative to the normal state as a function of the applied magnetic field. This data extracted from each MFMMS scans at different fields. A drastic increase in the MFMMS signal is found close to the 800 Oe applied field.

5.1.2. MgB_2. Superconductivity in MgB_2 at 39 K [109] shows two superconducting gaps with similar properties to phonon-mediated type II superconductors. Microwave absorption measurements have been used in the past to measure the penetration depth and surface impedance dependencies as a function of temperature [110]. Polycrystalline MgB_2 and high-T_c superconductivity materials were compared using similar techniques [111]. The power absorption was mainly attributed

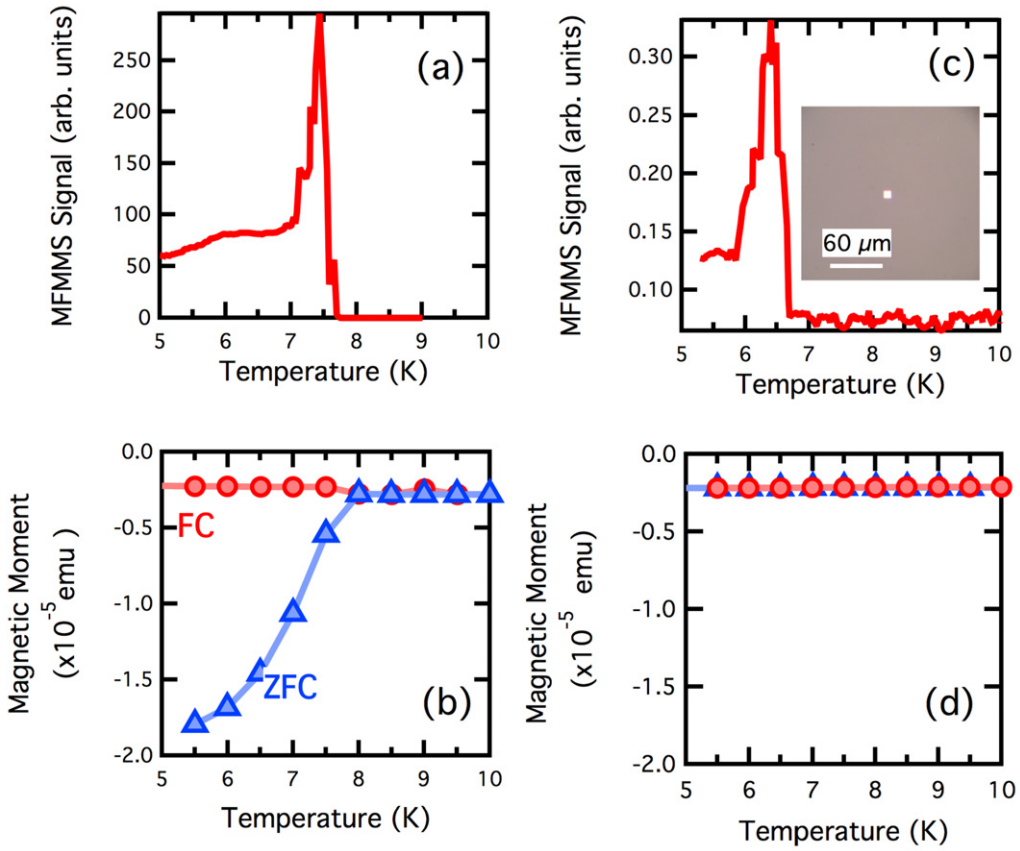

Figure 15. (*a*) MFMMS signal for a 100 nm thick Nb continuous film and the corresponding magnetization measurement (*b*). Blue triangles and circles indicate ZFC and FC curves, respectively. (*c*) MFMMS signal for a $10 \times 10\,\mu m^2$ patterned Nb sample with the same thickness. Inset shows an optical microscope image of the Nb square (white). (*d*) The corresponding magnetization measurement for the patterned sample. SQUID signal is in the noise level and there is no separation between ZFC-FC branches.

Table 2. List of various phase transitions studied by MFMMS.

Sample	Type	Form	Transition	$T_c^\mu / T_N / T_{curie}$ (K)
Nb (MBE)	Element	Thin film	SC	9.4
Nb (Sputtered)	Element	Thin film	SC	8.8
Nb (Patterned)	Element	Thin film	SC	7.6
MgB_2	Boride	Powder	SC	36.7
$ErRh_4B_4$	Boride	Single crystal [96]	SC	8.7
$FeTe_{0.65}Se_{0.35}$	Pnictide	Single crystal [97]	SC	14
$YBa_2Cu_3O_{7-x}$	Cuprate	Powder/film [60]	SC	89
$Bi_2Sr_2CuO_{8+x}$	Cuprate	Single crystal	SC	90
$Pr_xGd_{1-x}Ba_2Cu_3O_7$	Cuprate	Thin films [61]	SC	78
$GdBa_2Cu_3O_{9-y}$	Cuprate	Powder	SC	90
Mo–Sr–Eu–Cu–O	Cuprate	Singlecrystal	SC	33
La_2C_{3-x}	Carbide	Powder [6]	SC	6–8
MnO	—	Powder	AF-MIT	120
$FeCl_2$	—	Powder	AF[a]	20
FeF_2	—	Powder	AF	80
Dy	—	Pellet	F, AF	85,179
$PrSi_2$	—	Bulk [98]	F	∼10
Gd	—	Pellet	F	290
NiS	—	Powder	AF-MIT	260
V_2O_3	—	Powder	AF-MIT	150

[a] Metamagnetic transition. AF-MIT: antiferromagnetic transition coupled to a metal–insulator transition. F: ferromagnetic transition. SC: superconducting transition.

to coupled Josephson junctions with large effective penetration depth. The decrease in grain size causes an increase in surface resistance.

Figure 16(*d*) shows the MFMMS signal of MgB_2 with 15 Oe applied magnetic field. The transition temperature T_c^μ and the maximum signal relative to the normal state ($S_{max} - S_n$)

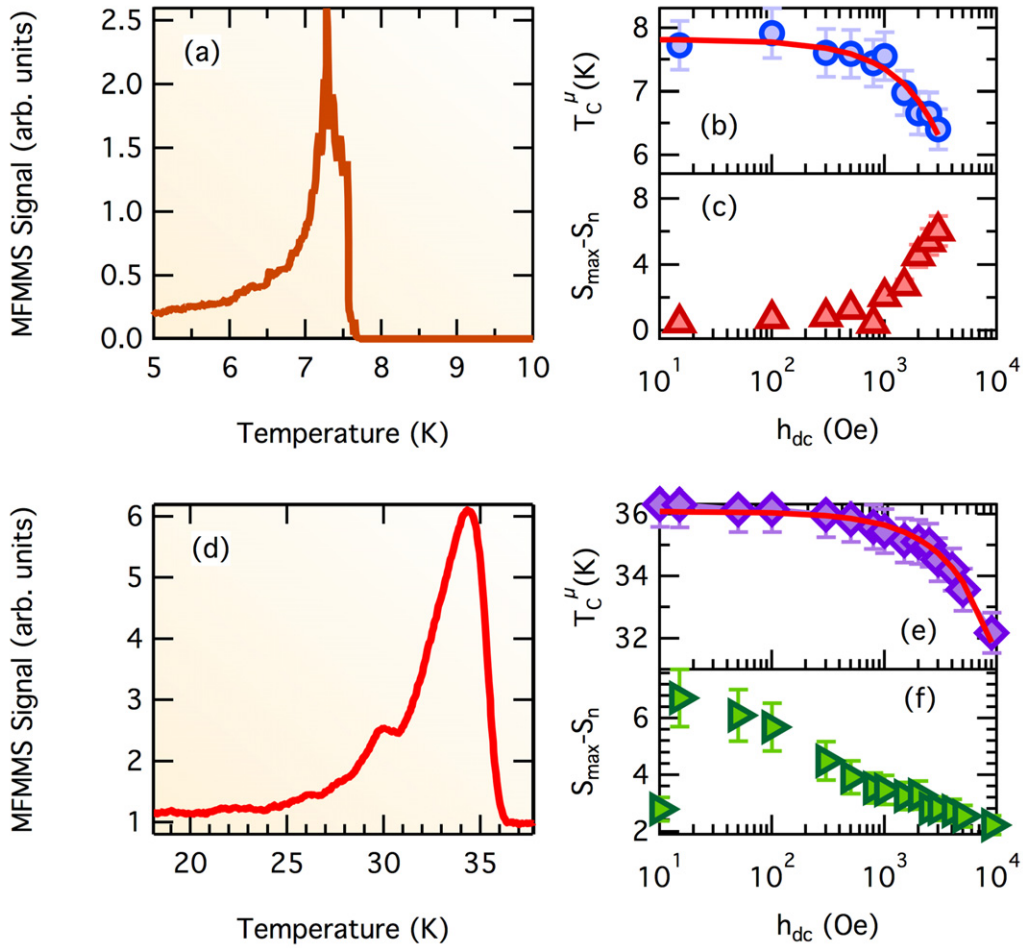

Figure 16. MFMMS measurement for single crystal $ErRh_4B_4$ (*a*) and stoichiometric powders of MgB_2 (*d*). Obtained T_c^{μ} at different dc magnetic fields for $ErRh_4B_4$ (*b*) and MgB_2 (*e*). The red solid line in both figures is fit to equation (7). Maximum MFMMS signal intensity at each magnetic field for $ErRh_4B_4$ (*c*) and MgB_2 (*f*). Note the logarithmic scale on the horizontal axis in (*b*), (*c*), (*e*) and (*f*).

are plotted as a function of magnetic field in figures 16(*e*) and (*f*), respectively. The T_c (36 K) and h_{c2} (40 kOe) extracted from the fit to equation (7) are in agreement with earlier reports [112, 113].

The relative change of MFMMS signal as a function of applied magnetic field for $ErRh_4B_4$ and MgB_2 seems to show opposite trends. The superconducting properties for each particular material need to be considered to explain this magnetic field dependence. In fact, the MFMMS signal should be suppressed for applied magnetic fields more than the critical field h_{c2}. For fields below h_{c2}, this behavior is governed by the specific superconducting properties of each material.

5.2. MFMMS across non-superconducting transitions

5.2.1. Antiferromagnetic–paramagnetic. The magnetic susceptibility considerably increases for a typical antiferromagnetic (AF) transition at the Neél temperature T_N [114]. This suggests that the microwave absorption should vary nonlinearly [17] and produces a non-zero MFMMS signal. We investigate MnO, a well-known antiferromagnet ($T_N = 116$ K) [115], to study MFMMS response for antiferromagnetic transition (figure 17(*a*)). The measurement was recorded with 100 Oe dc magnetic field, 15 Oe ac field amplitude and 1 mW microwave power. MFMMS signal increases below 200 K and reaches a maximum at 140 K. A decrease of almost 80% of the signal occurs between 140 and 120 K and following a plateau that extends to 5 K (shown only down to 50 K). The MFMMS signal is larger in the paramagnetic state than below the magnetic ordering temperature (T_N). No sharp peak-like behavior was observed at any temperature. For comparison, magnetization as a function of temperature from a SQUID magnetometer is included in figure 17(*b*). The change in the magnetization associated with antiferromagnetic transition obtained from SQUID is in agreement with MFMMS.

This behavior can be explained considering that nonlinear changes in the magnetic moments (or in the magnetic permeability) in MnO induce a non-monotonic behavior of the surface resistance, giving rise to the change in MFMMS signal. It is important to note that we also investigate the antiferromagnetic transition in V_2O_3 (shown in section 5.2.3), as another example. There is no significant change in MFMMS signal for V_2O_3 across the antiferromagnetic transition. This indicates the complex nature of dependence of microwave absorption across non-superconducting transitions and suggests evaluating each individual case rather than generalizing.

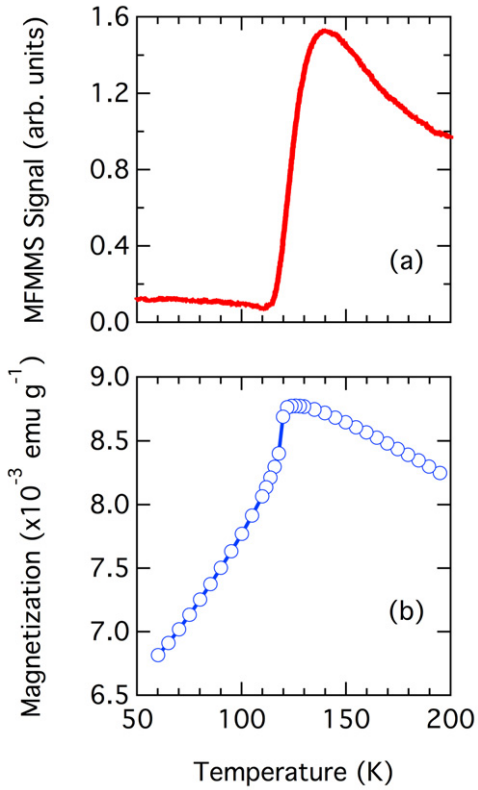

Figure 17. (*a*) MFMMS signal across antiferromagnetic transition of MnO powders at $h_{dc} = 15$ Oe. (*b*) Magnetization as a function of temperature at $h_{dc} = 15$ Oe. The temperature is swept from 50 to 200 K in both measurements.

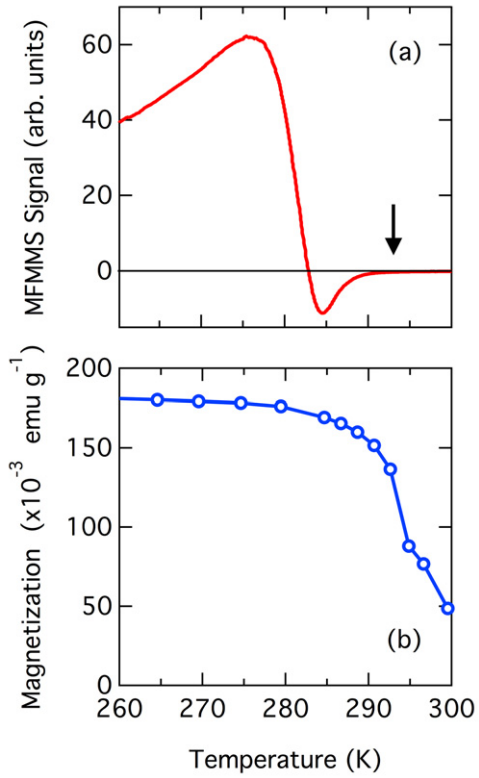

Figure 18. (*a*) MFMMS signal as a function of temperature for a ferromagnetic sublimated Gd. The arrow shows the onset of the ferromagnetic transition. (*b*) SQUID measurement of magnetization as a function of temperature. In both cases, the applied magnetic field was 15 Oe.

5.2.2. Ferromagnetic–paramagnetic. Similarly, it is expected that the ferromagnetic (FM) transitions produce MFMMS signals. Microwave absorption, in particular the shape of the MFMMS signal, is not correlated only with changes in the magnetic moments or magnetic permeability. Magnetoresistive effects need to be considered in order to understand MFMMS from ferromagnets [116]. In this section, we examine two prototypical examples of ferromagnetic transitions in Gd and $PrSi_2$.

5.2.2.1. Gadolinium. The magnetic properties of Gd have been widely studied. Gd has the highest magnetic ordering temperature among the rare earth elements ($T_{Curie} = 294$ K) [117]. The magnetic ordering involves changes in the resistivity ρ (T) and magnetic permeability μ (T).

The MFMMS measurement is presented in figure 18(*a*). The MFMMS signal deviates from zero at around 294 K, indicating the onset of the ferromagnetic transition. As the temperature decreases below T_{Curie}, a minimum and maximum occur at 285 K and 275 K respectively. Figure 18(*b*) shows magnetization as a function of temperature for the same sample. The T_{Curie} value measured by MFMMS coincides with the middle of the magnetic transition, around 294 K showing that the change in the MFMMS signal is produced by the magnetic ordering of Gd [17]. More precise determination of the T_{Curie} temperature from SQUID will require the use of Arrott plots [118].

It is important to note that although the MFMMS signal increases for the ferromagnetic transition in Gd, the signal shape and magnetic field dependency are different than superconducting transitions. More details will be given in section 6.

5.2.2.2. $PrSi_2$. Figure 19 shows the MFMMS (*a*) and SQUID (*b*) data for bulk $PrSi_2$ alloy prepared by arc-melting [98]. The ferromagnetic transition at 11 K is confirmed by the two measurements. The ferromagnetic transition appears as a sharp dip in the MFMMS signal. This is a unique case that the signal has opposite phase in comparison with superconducting transitions. Having opposite phases is confirmed by mixing $PrSi_2$ with a well-known superconductor (Pb, data not shown). Similar MFMMS results have been recently reported from partially oxidized CuCl [119].

5.2.3. Metal–insulator transitions. Vanadium sesquioxide (V_2O_3) undergoes a temperature-induced metal–insulator (MIT) at $T_{MIT} \approx 150$–160 K depending on the oxygen stoichiometry. This is accompanied by a change in the crystal symmetry from monoclinic to rhombohedral and magnetically from paramagnetic to antiferromagnetic phase [120]. Stoichiometric V_2O_3 powders were studied for the microwave absorption across MIT transitions.

Figure 20(*a*) depicts the MFMMS data measured with $h_{dc} = 100$ Oe, $h_{ac} = 15$ Oe, and 1 mW microwave

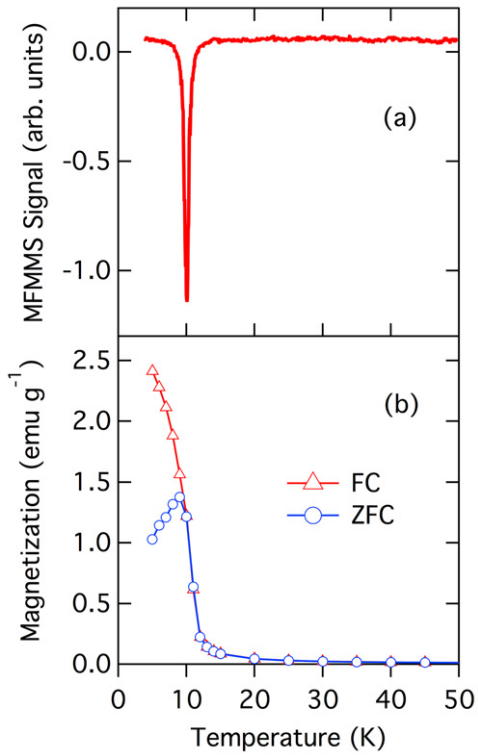

Figure 19. (*a*) MFMMS signal as a function of temperature across ferromagnetic transition of $PrSi_2$ powder. (*b*) ZFC-FC measurement of the same sample. Note the MFMMS signal shows a dip at the transition. Figure adapted from [98].

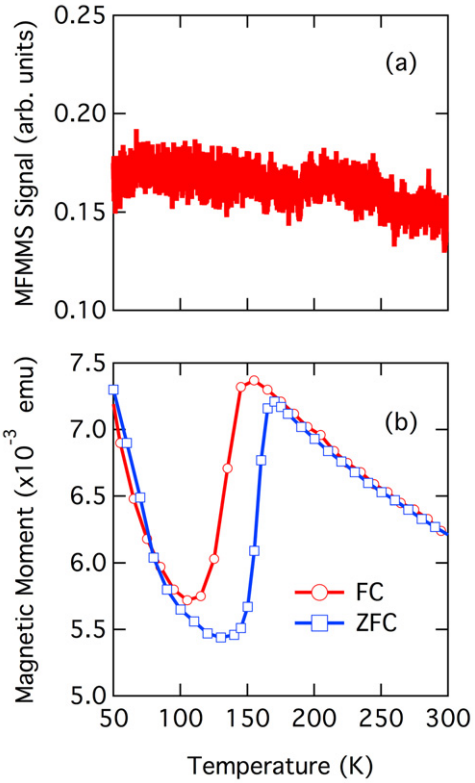

Figure 20. (*a*) MFMMS signal as a function of temperature of V_2O_3 powders at $h_{dc} = 100$ Oe. (*b*) ZFC-FC magnetization curves with 100 Oe applied field.

power. The MFMMS signal is at the noise level through the whole temperature range and shows no significant change. Figure 20(*b*) shows the corresponding ZFC-FC magnetization measurement from SQUID magnetometry. The antiferromagnetic transition (AF) and hysteretic behavior between cooling and heating branches are clearly visible in the magnetometry measurements.

Despite the change in magnetization and resistance of the material (the resistance increases by approximately seven orders of magnitude) [121], the MFMMS signal does not show any feature. This absence of MFMMS signal has been reported previously [59]. It was argued that the weak magnetic response of V_2O_3 prevents the absorption from being modulated. Therefore, the phase locked signal is not detected by MFMMS. The change of the local moment across the metal–insulator transition is close to 10% (1.3 Bohr magnetons per Vanadium atom in the insulating state and 1.2 Bohr magnetons in the metallic state [122]).

5.2.4. Paramagnetic–metamagnetic. Although metamagnets show an increase in magnetization as a function of field, they are not classified as an antiferromagnet, ferrimagnet, or ferromagnet—see for example [123] and references therein. These types of transitions are of special interest to address the selectivity of superconducting transitions by the MFMMS technique. It combines AF and FM-like behavior depending on the external magnetic field applied. A typical case of metamagnetic material is $FeCl_2$. It behaves like an antiferromagnetic material below $T_N \sim 23$ K. The metamagnetic transition occurs within this temperature range. As the magnetic field is increased, the material undergoes a transition from a low-moment and low-susceptibility to a high-moment and high-susceptibility state. A list of materials that exhibit metamagnetic transitions was shown in a detailed review [124].

We studied the metamagnetic transition of $FeCl_2$ powders by measuring MFMMS as a function of temperature at different applied fields (figure 21(*a*)). The temperature is always swept downwards from 60 to 5 K. It was found that the temperature at which the signal is zero (20 K) is independent of applied field. Figure 21(*b*) shows the hysteretic behavior of MFMMS measurements when the temperature is swept up and down, for $h_{dc} = 3$ kOe. Figure 21(*c*) depicts SQUID measurements for the same sample. The transition temperature is in good agreement with MFMMS data, and a hysteretic behavior between ZFC-FC branches is also present.

The hysteretic behavior of this material has been used in previous works to support the idea that the metamagnetic transition in $FeCl_2$ is first order [123, 125, 126]. The MFMMS data from $FeCl_2$ shows features that are similar to both ferromagnetic transitions and AF transitions, i.e. the hysteresis upon heating and cooling and the reduction of the microwave absorption below the Néel temperature, respectively.

6. Selectivity of the MFMMS technique

Low field microwave absorption (LFMA) consists of the measurements of the modulated microwave absorption across

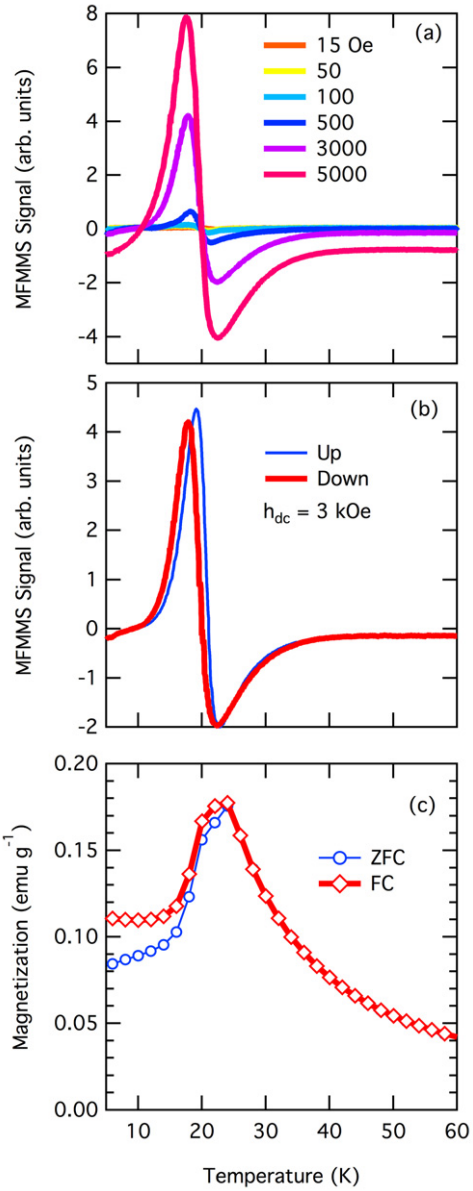

Figure 21. (*a*) MFMMS signal as a function of temperature for $FeCl_2$ powder at different applied magnetic fields, h_{dc}. (*b*) Hysteresis of MFMMS curves for 3 kOe applied field. Sweeping up (blue, thicker line) and down (red, thinner line). (*c*) ZFC and FC SQUID measurements of the same sample as a function of temperature at $h_{dc} = 3$ kOe.

a small range of fields around zero. LFMA has been measured in a number of systems, from superconductors to ferromagnets [8, 55, 70, 74, 112, 116, 127–129]. For a superconducting sample, the field-derivative of the microwave absorption shows a large hysteresis between upward and downward dc field sweeps. The hysteresis was attributed to the existence of weakly coupled superconducting clusters (grains) [56, 130]. In general, the measured signal can be considered to be the field derivative of the imaginary part of the magnetic susceptibility. The detailed interpretation of these measurements is out of the scope of this review and is described in [131].

LFMA measurement of MgB_2 at 35 K using the MFMMS setup is shown in figure 22(*a*). The dc field was ramped from −100 up to 100 Oe (blue dashed line) and then ramped

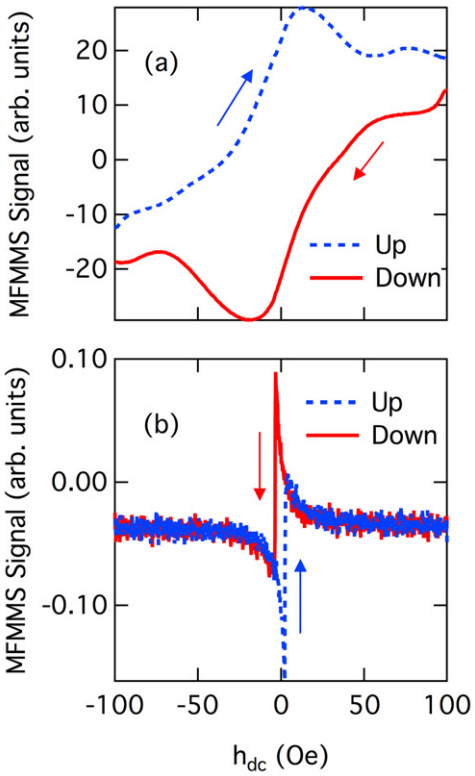

Figure 22. MFMMS versus field. Field sweep up (blue dash) and field sweep down (red solid) for: (*a*) MgB_2 powder at 35 K and (*b*) Py 100 nm thick film at 100 K. Vertical line on (*a*) indicates the maximum MFMMS signal at 15 Oe.

back to −100 Oe (red solid line) at a rate of 1 Oe s^{-1}. Note that the signal is larger when sweeping the magnetic field upwards. Except the exact shape of the signal and corresponding magnetic field values, similar hysteretic behavior is reproducible for all superconducting samples measured below T_c^{μ}. This hysteretic behavior completely disappears above T_c^{μ}.

LFMA measurement of a permalloy (Py) thin film at 300 K is shown in figure 22(*b*). The signal shows a sharp minimum at $h_{dc} = 4$ Oe when the magnetic field was swept upwards and reaches the background level at 20 Oe. When the field was swept downwards, the signal had an opposite trend. This behavior has been attributed to a ferromagnetic resonance of individual ferromagnetic domains prior to saturation [116, 129].

It is important to note that when sweeping the magnetic field, the MFMMS signal of Py and MgB_2 shows opposite trends; the former has a minimum in the MFMMS signal while the latter has a maximum for upwards scans. This trend was confirmed for all measured superconducting and ferromagnetic samples. This behavior can be explained considering that superconducting materials exhibit a diamagnetic response to the applied field while FM materials have the opposite response [132]. These results show that LFMA can be used as a tool to differentiate ferromagnetic and superconducting phase transitions. For further reading about LFMA we refer to [133] and [116] for the case of superconductors and ferromagnetic materials, respectively.

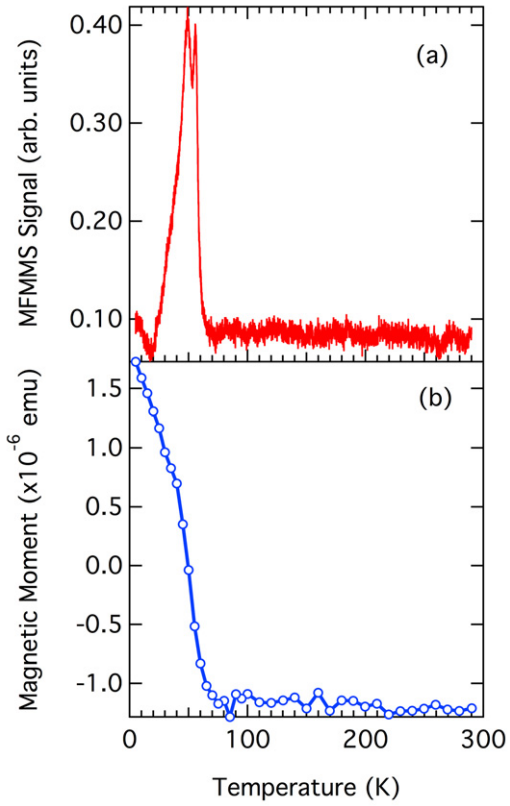

Figure 23. (*a*) MFMMS and (*b*) magnetization measurements as a function of temperature for single crystal GaMnAs.

As a further test, we measured a ferromagnetic insulator, GaMnAs. The MFMMS signal from insulating ferromagnets can be confused with a superconducting transition, since both produce a peak like response. This is due to the relative change of the magnetic susceptibility with respect to the ac conductivity, which defines the surface resistance R_s. In figure 23, we show the MFMMS (*a*) and SQUID (*b*) measurements of a GaMnAs single crystal. The MFMMS signal appears as a clear peak at the transition. In order to distinguish this peak-like behavior from a superconducting transition, the field-dependent absorption (LFMA) below the critical temperature can be measured. GaMnAs single crystal field sweeps are similar to those shown for Py in figure 23(*b*). This suggests that in cases where the material is unknown, a combination of MFMMS and LFMA measurements can differentiate between superconductors and ferromagnets.

In summary, if a MFMMS spectrum shows any abrupt changes during the temperature sweep, additional low field scans can distinguish the nature of the transition. Superconducting transitions have a unique signature and can easily be distinguished from other types of transitions, as mentioned above.

7. Route for new superconductors

The search for new superconductors is akin to finding a 'needle in a haystack', in which most of the material is irrelevant. Therefore, it is important to develop an efficient method to discard the 'uninteresting' parts of the phase diagram. 'Interesting' phases are sometimes not in thermodynamic equilibrium, and can only be stabilized through specialized synthesis routes. It is important to point out that, in many cases, the first available samples of superconducting materials are likely to be multiphase. This calls for a method through which most of the non-superconducting materials could be efficiently discarded, leading to the idea that the following two ingredients are crucial for the search of new materials: (1) synthesis by as many preparation methods as possible, and (2) fast, sensitive and efficient methods that allow discarding of large parts of the phase diagram which are not of interest. Further restrictions have to be placed on the systems to be investigated; otherwise the number of systems becomes intractable. These additional restrictions can be obtained from theoretical input or from qualitative ideas based on observations and guided by chemical and material science intuition. This general philosophy could be applied to many desired physical phenomena, but is particularly well suited for the search for new superconductors.

There are very few general guidelines which can be extracted from past experience. It is possibly safe to assume that future discoveries will arise in multi-element compounds, as proven by the recent discovery of superconductivity in the pnictides, although even binary alloys (such as magnesium diboride) went unnoticed for a long time. In most cases, the high temperature superconductors contain light elements such as (B, C, N, O, F, S, Cl). Moreover, charge separation among substructures in the material appears, so that both ionic and metallic/co-valent bonding exists side by side, as for instance in layered compounds. Perhaps the proximity to a magnetic and/or metal insulator behavior may also serve as further help in restricting the large phase space available for search. Attempts at doping these may yield the results we are seeking. The problem is that to satisfy simultaneously all conditions outlined above is nontrivial and therefore one may want to start from compounds which partially satisfy some of the conditions.

8. Conclusions

MFMMS can be used as a fast, sensitive and selective technique to search for the presence of superconductivity. MFMMS is a high-sensitivity technique capable of detecting volumes of superconducting phases as small as 10^{-12} cm^3 even in discontinuous samples, which we demonstrated by patterning a Nb film. The signature of superconductivity is a drastic change in the field derivative of the microwave power absorbed at the transition temperature. The dependence of the MFMMS signal on the field parameters (h_{ac}, h_{dc} and h_{rf}) enables the determination of h_{c2} and the transition temperatures. It has been shown that the technique is able to detect multiple superconducting phases in the same material, with different T_c. Further investigation is needed to quantitatively understand the MFMMS signal.

We showed that superconducting transitions can be separated from other phase transitions using LFMA in addition to MFMMS measurements. The correlation between MFMMS, dc magnetization, and resistivity shows a route for

the identification of unknown phases. This technique, together with new synthesis methods—particularly the growth of new materials using combinatorial techniques—can play a crucial role in the search for new superconductors.

Acknowledgments

We thank Ralph Weber for his support with the customization of the EPR system and discussion of the results at the initial stage of this work. We thank Z Fisk, P D Esquinazi, D Hinks, G Larkins, R Puzniak, M Beasley, S Risbud, T J Haugan, M A Alario-Franco, D Basov, J Sonier, P Guptasarma, O Shpyrko, J Hirsch, K Dumesnil, J Villegas, and B Maple for providing interesting samples at different stages of this work. Special thanks to H Weinstock for continuous support and critical suggestions. Research supported by an AFOSR MURI grant FA49550-09-1-0577.

References

[1] Schrieffer J and Tinkham M 1999 Superconductivity *Rev. Mod. Phys.* **71** S313–7
[2] Bardeen J, Cooper L N and Schrieffer J R 1957 Theory of superconductivity *Phys. Rev.* **108** 1175–204
[3] Bednorz J G and Muller K A 1986 Possible high T_c superconductivity in the Ba–La–Cu–O system *Z. Phys.* B **64** 189–93
[4] Stewart G R 2011 Superconductivity in iron compounds *Rev. Mod. Phys.* **83** 1589–652
[5] Hirschfeld P J, Korshunov M M and Mazin I I 2011 Gap symmetry and structure of Fe-based superconductors *Rep. Prog. Phys.* **74** 124508
[6] de la Venta J, Basaran A C, Grant T, Machado A J S, Suchomel M R, Weber R T, Fisk Z and Schuller I K 2011 Methodology and search for superconductivity in the La–Si–C system *Supercond. Sci. Technol.* **24** 075017
[7] Hardy W, Bonn D, Morgan D, Liang R and Zhang K 1993 Precision measurements of the temperature dependence of λ in $YBa_2Cu_3O_{6.95}$: strong evidence for nodes in the gap function *Phys. Rev. Lett.* **70** 3999–4002
[8] Topagh C 1996 Modulated microwave absorption in $PbBi_2Sr_2Ca_2Cu_3O_y$ powders and possible flux melting *J. Supercond.* **9** 263–7
[9] Biondi M and Garfunkel M 1959 Measurement of the temperature variation of the energy gap in superconducting aluminum *Phys. Rev. Lett.* **2** 143–5
[10] Gould A, Jackson E M, Renouard K, Crittenden R, Bhagat S M, Spencer N D, Dolhert L E and Wormsbecher R F 1988 Grain-size dependence of microwave-absorption in $Y_1Ba_2Cu_3O_7$ powders near T_c *Physica* C **156** 555–8
[11] Biondi M, Forrester A, Garfunkel M and Satterthwaite C 1958 Experimental evidence for an energy gap in superconductors *Rev. Mod. Phys.* **30** 1109–36
[12] Jackson E M, Liao S B, Silvis J, Swihart A H, Bhagat S M, Crittenden R, Glover R E and Manheimer M A 1988 Initial susceptibility and microwave absorption in powder samples of $Y_1Ba_2Cu_3O_{6.9}$ *Physica* C **152** 125–9
[13] Maeda A, Kitano H and Inoue R 2005 Microwave conductivities of high-T_c oxide superconductors and related materials *J. Phys.: Condens. Matter* **17** R143–85
[14] Gould A, Tyagi S D, Bhagat S M and Manheimer M A 1989 Grain size dependence of low field microwave absorption in $Y_1Ba_2Cu_3O_7$ powders *IEEE Trans. Magn.* **25** 3224–6
[15] Manheimer M A, Lofland S, Gould A, Bhagat S M, Halsey B, Green S M and Tyagi S 1991 Enhanced microwave absorption near T_c in micron-size powders of cuprate superconductors *Physica* C **183** 324–32
[16] Takano Y, Takeya H, Fujii H, Kumakura H, Hatano T, Togano K, Kito H and Ihara H 2001 Superconducting properties of MgB_2 bulk materials prepared by high-pressure sintering *Appl. Phys. Lett.* **78** 2914–6
[17] Owens F J and Poole C P Jr 1999 *Electromagnetic Absorption in the Copper Oxide Superconductors* (New York: Kluwer)
[18] Dulčić A, Crepeau R H, Freed J H, Schneemeyer L F and Waszczak J V 1990 Weak-link structure in $YBa_2Cu_3O_7$ single crystals: a microwave study *Phys. Rev.* B **42** 2155–60
[19] Tea N H, Salamon M B, Datta T, Duan H M and Hermann A M 1992 Field-modulated microwave surface resistance in a single-crystal $Tl_2Ca_2BaCu_2O_8$ superconductor *Phys. Rev.* B **45** 5628–32
[20] Gough C E and Exon N J 1994 Microwave response of anisotropic high-temperature-superconductor crystals *Phys. Rev.* B **50** 488–95
[21] Nefyodov Y A, Shuvaev A M and Trunin M R 2007 Microwave response of V_3Si single crystals: evidence for two-gap superconductivity *Europhys. Lett.* **72** 638–44
[22] Panina L V and Mohri K 1994 Magneto-impedance effect in amorphous wires *Appl. Phys. Lett.* **65** 1189–91
[23] Biondi M, Garfunkel M and McCoubrey A 1957 Microwave measurements of the energy gap in superconducting aluminum *Phys. Rev.* **108** 495–7
[24] Coffey M and Clem J 1991 Unified theory of effects of vortex pinning and flux creep upon the rf surface impedance of type-II superconductors *Phys. Rev. Lett.* **67** 386–9
[25] Wingfield J J, Powell J R, Gough C E and Porch A 1997 Sensitive measurement of the surface impedance of superconducting single crystals using a sapphire dielectric resonator *IEEE Trans. Appl. Supercond.* **7** 2009–12
[26] Huttema W A, Morgan B, Turner P J, Hardy W N, Zhou X, Bonn D A, Liang R and Broun D M 2006 Apparatus for high-resolution microwave spectroscopy in strong magnetic fields *Rev. Sci. Instrum.* **77** 023901
[27] Bonura M, Agliolo Gallitto A, Li Vigni M and Martinelli A 2008 Depinning frequency in a heavily neutron-irradiated MgB_2 sample *Physica* C **468** 2372–7
[28] Gough C E, Ormeno R J, Hein M A, Sibley A, Wingfield J J, Powell J, Porch A, Yang G, Maeno Y and Mao Z Q 2001 The low temperature microwave properties of $GdBa_2Cu_3O_{7-\delta}$ and Sr_2RuO_4 *J. Supercond.* **14** 73–9
[29] Sridhar S and Mercereau J E 1986 Nonequilibrium dynamics of quasiparticles in superconductors *Phys. Rev.* B **34** 203–16
[30] Sridhar S and Kennedy W L 1988 Novel technique to measure the microwave response of high T_c superconductors between 4.2 and 200 K *Rev. Sci. Instrum.* **59** 531–6
[31] Dietl L and Trinks U 1989 The surface resistance of a superconducting lead–tin alloy *Nucl. Instrum. Methods* A **284** 293–5
[32] Baker P J, Ormeno R J, Gough C E and Fisher I R 2010 Microwave surface impedance measurements of $Tl_xPb_{1-x}Te$: a proposed negative-U induced superconductor *Phys. Rev.* B **81** 064506
[33] Truncik C J S *et al* 2013 Nodal quasiparticle dynamics in the heavy fermion superconductor $CeCoIn_5$ revealed by precision microwave spectroscopy *Nature Commun.* **4** 2477
[34] Dressel M, Klein O, Donovan S and Grüner G 1993 Microwave cavity perturbation technique: III. Applications *Int. J. Infrared Millim.* **14** 2489–517
[35] Donovan S, Klein O, Dressel M, Holczer K and Grüner G 1993 Microwave cavity perturbation technique: II. Experimental scheme *Int. J. Infrared Millim.* **14** 2459–87

[36] Klein O, Donovan S, Dressel M and Grüner G 1993 Microwave cavity perturbation technique: I. Principles *Int. J. Infrared Millim.* **14** 2423–57

[37] Peligrad D N, Nebendahl B, Kessler C, Mehring M, Dulčicì A, Požek M and Paar D 1998 Cavity perturbation by superconducting films in microwave magnetic and electric fields *Phys. Rev.* B **58** 11652–71

[38] Jackson E M, Shaw G J, Crittenden R, LI Z Y, Stewart A M, Bhagat S M and Glover R E 1989 Study of microwave-power absorption in yttrium barium copper based high-temperature superconductors and allied compounds *Supercond. Sci. Technol.* **2** 29–34

[39] Aktaş B and Zafer Durusoy H 1996 A new technique for measuring the microwave penetration depth in high-T_c superconducting thin films *Physica* C **260** 81–5

[40] Stankowski J and Czyźak B 1991 Microwave absorption in high-T_c superconductors studied by the EPR method *Appl. Magn. Reson.* **2** 465–79

[41] Portis A M, Blazey K W, Muller K A and Bednorz J G 1988 Microwave magnetosurface impedance of high-T_c superconductors *Europhys. Lett.* **5** 467–72

[42] Požek M, Dulčicì A and Rakvin B 1990 Field-modulated microwave absorption in granular superconductors: first and second harmonic signals *Physica* C **169** 95–9

[43] Mahe' M and Beňačka Š 1992 Modulated microwave absorption in superconductors *Solid State Commun.* **83** 615–8

[44] Demidov V V and Noginova N E 1992 Modulated radiofrequency and microwave absorption in superconductors with intrinsic weak links *Solid State Commun.* **82** 527–9

[45] Dulčicì A, Leontić B, Perić M and Rakvin B 1987 Microwave study of Josephson junctions in Gd–Ba–Cu–O compounds *Europhys. Lett.* **4** 1403–7

[46] Khachaturyan K, Weber E R, Tejedor P, Stacy A M and Portis A M 1987 Microwave observation of magnetic field penetration of high-T_c superconducting oxides *Phys. Rev.* B **36** 8309–14

[47] Blazey K W, Muller K A, Bednorz J G, Berlinger W, Amoretti G, Buluggiu E, Vera A and Matacotta F C 1987 Low-field microwave-absorption in the superconducting copper oxides *Phys. Rev.* B **36** 7241–3

[48] Blazey K W, Portis A M and Bednorz J G 1988 Microwave study of the critical state in high-T_c superconductors *Solid State Commun.* **65** 1153–6

[49] Andrzejewski B, Czyźak B, Szczesniak L and Stankowski J 1995 Lower Josephson critical-field in granular HTS measured by microwave-absorption *Appl. Magn. Reson.* **8** 35–44

[50] Chen J, Wenger L, McEwan C and Logothetis E 1987 Observation of the reverse ac Josephson effect in Y–Ba–Cu–O at 240 K *Phys. Rev. Lett.* **58** 1972–5

[51] Tsai J, Kubo Y and Tabuchi J 1987 Josephson effects in the Ba–Y–Cu–O compounds *Phys. Rev. Lett.* **58** 1979–81

[52] Estève D, Martinis J M, Urbina C, Devoret M H, Collin G, Monod P, Ribault M and Revcolevschi A 1987 Observation of the a.c. Josephson effect inside copper-oxide-based superconductors *Europhys. Lett.* **3** 1237–42

[53] Kheifets A S and Veinger A I 1990 Low-field microwave absorption and quantum oscillations in type-I superconductors *Physica* C **165** 491–8

[54] Shaposhnikova T, Talanov Y and Vashakidze Y 2003 Origin of the irreversible microwave absorption versus the state of vortex matter in $Bi_2Sr_2CaCu_2O_x$ single crystals *Physica* C **385** 383–92

[55] Panarina N Y, Talanov Y I, Shaposhnikova T S, Beysengulov N R and Vavilova E 2010 Pinning effects in ceramic $SmO_{1-x}F_xFeAs$ as revealed by microwave absorption *Phys. Rev.* B **81** 224509

[56] Karim R, Oliver S, Vittoria C, Widom A, Balestrino G, Barbanera S and Paroli P 1989 Low-field dependence of the microwave absorption in superconducting $YBa_2Cu_3O_{7-x}$ near T_c *Phys. Rev.* B **39** 797–800

[57] Stankowski J and Czyżak B 1993 Tester for granular superconductors *Rev. Sci. Instrum.* **64** 2930–2

[58] Wijeratne A T, Dunifer G L, Chen J T, Wenger L E and Logothetis E M 1988 Millimeter-wave absorption in La–Ba–Cu–O and Y–Ba–Cu–O superconductors *Phys. Rev.* B **37** 615–8

[59] Kim B F, Bohandy J J, Mooriani K and Adrian F J 1988 A novel microwave technique for detection of superconductivity *J. Appl. Phys.* **63** 2029–32

[60] Chan I N, Vier D C, Nakamura O, Hasen J, Guimpel J, Schultz S and Schuller I K 1993 Thickness dependence of the superconducting transition temperature of YBCO *Phys. Lett.* A **175** 241–5

[61] Lederman D, Vier D C, Mendoza D, Santamaria J, Schultz S and Schuller I K 1995 Detection of new superconductors using phase-spread alloy-films *Appl. Phys. Lett.* **66** 3677–9

[62] Knigge B, Hoffmann A, Lederman D, Vier D C, Schultz S and Schuller I K 1997 Search for new superconductors in the Y–Ni–B–C system *J. Appl. Phys.* **81** 2291–5

[63] Shaltiel D, Bill H, Grayevsky A, Junod A, Lovy D, Sadowski W and Walker E 1991 Microwave absorption across T_c: determination of the angular dependence $H_{c2}(\theta)/H_{c2}$ *Phys. Rev.* B **43** 13594–7

[64] Martinek J and Stankowski J 1995 Magnetically modulated microwave-absorption in twin boundaries of a high-temperature superconducting single-crystal *Appl. Magn. Reson.* **8** 89–97

[65] Czyźak B, Andrzejewski B, Szczesniak L, Danilova N and Stankowski J 1995 Periodic microwave-absorption in superconducting whiskers *Appl. Magn. Reson.* **8** 25–33

[66] Likodimos V and Pissas M 2002 Electron spin resonance and microwave absorption study of MgB_2 *Phys. Rev.* B **65** 172507

[67] Piekara-Sady L, Jurga W, Kempiński W, Łoś S, Stankowski J, Piekoszewski J, Barlak M, Werner Z and Stanislawski J 2008 Magnetically modulated microwave absorption study of superconducting MgB_2 regions *Appl. Magn. Reson.* **34** 157–62

[68] Bele P, Brunner H, Schweitzer D and Keller H J 1994 Magnetically modulated microwave absorption (MMMA) at low magnetic fields in (BEDT-TTF)-superconductors *Solid State Commun.* **92** 189–93

[69] Andrzejewski B, Guilmeau E and Kowalczyk A 2008 The effect of structure on flux instability and on the superconducting properties of the $Mo_2Re_3B_x - Mo_3Re_2B_x$ eutectic *Supercond. Sci. Technol.* **21** 045008

[70] Stankowski J, Stobiecki F and Gorska M 2003 Application of magnetically modulated microwave absorption to study of giant magnetoresistance effect in the Ni–Fe/Cu multilayer system *Appl. Magn. Reson.* **24** 303–11

[71] Tyagi S 1995 Magnetically modulated microwave absorption in cuprate superconductors *Appl. Magn. Reson.* **8** 147–55

[72] Khairullin I L, Khabibullaev P K, Sokolov V Y and Zakhidov A A 1999 Low-magnetic field microwave absorption in superconductors and conducting polymers *Turk. J. Phys.* **23** 1107–26

[73] Rubins R, Hutton S, Drumheller J, Jeong D and Black T 1989 Noise in the microwave absorption of $YBa_2Cu_3O_{7-\delta}$ *Phys. Rev.* B **39** 2775–8

[74] Rubins R, Black T, Song K and Jeong D 1991 Modulation corrections to the modulated microwave absorption of a pure mercury sample *Phys. Rev.* B **43** 210–5

[75] Rubins R S, Hutton S L and Drumheller J E 1989 Microwave absorption of a superconducting lead sphere *Phys. Rev.* B **39** 4666–9

[76] Rubins R, Black T and Jeong D 1989 Modulated microwave absorption in superconducting mercury *Phys. Rev.* B **40** 2551–4

[77] Hebard A F, Rosseinsky M J, Haddon R C, Murphy D W, Glarum S H, Palstra T T M, Ramirez A P and Kortan A R 1991 Superconductivity at 18 K in potassium-doped C_{60} *Nature* **350** 600–1

[78] Glarum S, Schneemeyer L and Waszczak J 1990 Microwave loss and oxygen annealing in $YBa_2Cu_3O_x$ single crystals *Phys. Rev.* B **41** 1837–41

[79] Buluggiu E and Vera A 1997 Granular nature and superconductive coupling of $YBa_2Cu_3O_7$ polycrystals observed by microwave absorption measurements *J. Low Temp. Phys.* **106** 469–74

[80] Nebendahl B, Kessler C, Peligrad D N and Mehring M 1993 Comparative investigation of intrinsic Josephson contacts in Htc superconductors by modulated microwave-absorption measurements *Physica* C **209** 362–8

[81] Kaur M A, Kadam R M, Bhide M K, Rane M V, Babu Y, Sastry M D, Gopalakrishnan I K and Yakhmi J V 2001 Microwave absorption studies of diluted high-temperature superconductors: delineation of superconductor–insulator–superconductor and superconductor–normal–superconductor junctions *Phil. Mag.* B **81** 267–77

[82] Stankowski J, Andrzejewski B, Czyźak B and Hilczer W 1993 Influence of microwave power on magnetically modulated microwave absorption in a granular high-temperature superconductor *Physica* C **215** 167–72

[83] Shaltiel D, Ginodman V, Golosovsky M, Katz U, Boasson H, Gerhouser W and Fischer P 1992 Investigation of the magnetic field-induced microwave absorption across T_c in single crystals of $YBa_2Cu_3O_{7-\delta}$ and BiSrCaCuO *Physica* C **202** 303–20

[84] Haddon R C, Glarum S H, Chichester S V, Ramirez A P and Zimmerman N M 1991 Microwave-loss studies of organic superconductors *Phys. Rev.* B **43** 2642–7

[85] Haddon R C, Ramirez A P and Glarum S H 1994 Electron–electron interactions in organic superconductors *Adv. Mater.* **6** 316–22

[86] Kataev V, Winkel G, Knauf N, Gruetz A, Khomskii D, Wohlleben D, Crump W, Hahn J and Tebbe K F 1992 ESR study of the electronic properties of the new organic conductors κ-(BEDT-TTF)$_2$Cu[N(CN)$_2$]X, X = Br; I *Physica* B **179** 24–34

[87] Rouco A, Obradors X, Briático J, Tovar M, Piñol S, Fontcuberta J and Causa M T 1994 Two dimensional superconductivity in $Sm_{2-x}Ce_xCuO_{4-\delta}$: evidence from microwave absorption *Physica* C **235–240** 2027–8

[88] Bramley R, Stewart A M, Thompson J G and White J W 1992 Quantised microwave power absorption in high temperature superconductors *Mater. Chem. Phys.* **30** 183–6

[89] Veinger A I, Zabrodskii A G and Tisnek T V 1995 Use of magnetosensitive microwave absorption in a search for new superconducting phases *Supercond. Sci. Technol.* **8** 368–73

[90] Gutiérrez M P, Alvarez G, Montiel H, Zamorano R and Valenzuela R 2007 Study of the Verwey transition in magnetite by low field and magnetically modulated non-resonant microwave absorption *J. Magn. Magn. Mater.* **316** e738–40

[91] Alvarez G and Zamorano R 2004 Characteristics of the magnetosensitive non-resonant power absorption of microwave by magnetic materials *J. Alloys Compounds* **369** 231–4

[92] Kremer R K, Kanellakopulos B, Bele P, Brunner H and Neugebauer F A 1991 Weak ferromagnetism and magnetically modulated microwave absorption at low magnetic fields in 1,3,5-triphenyl-6-oxoverdazyl *Chem. Phys. Lett.* **230** 255–9

[93] Stankowski J 2004 Application of MMMA method: dispersed superconductors and magnetic nanolayers *Appl. Magn. Reson.* **27** 251–8

[94] Shrivastava K N 1991 Magnetic resonance in high-temperature superconductors *Phys. Rep.* **200** 51–82

[95] Poole C P Jr, Farach H A, Creswick R J and Prozorov R 2007 *Superconductivity* (London: Academic)

[96] DePuydt J, Dahlberg E and Hinks D 1986 Thermodynamic study of the competition between superconductivity and magnetism in $ErRh_4B_4$ *Phys. Rev. Lett.* **56** 165–8

[97] Wittlin A, Aleshkevych P, Przybylińska H, Gawryluk D J, Dłużewski P, Berkowski M, Puźniak R, Gutowska M U and Wiśniewski A 2012 Microstructural magnetic phases in superconducting $FeTe_{0.65}Se_{0.35}$ *Supercond. Sci. Technol.* **25** 065019

[98] de la Venta J, Basaran A C, Grant T, Gallardo-Amores J M, Ramirez J G, Alario-Franco M A, Fisk Z and Schuller I K 2013 Magnetism and the absence of superconductivity in the praseodymium–silicon system doped with carbon and boron *J. Magn. Magn. Mater.* **340** 27–31

[99] Matthias B T, Corenzwit E, Vandenberg J M and Barz H E 1977 High Superconducting transition temperatures of new rare earth ternary borides *Proc. Natl Acad. Sci. USA* **74** 1334–5

[100] Sinha S, Crabtree G, Hinks D and Mook H 1982 Study of coexistence of ferromagnetism and superconductivity in single-crystal $ErRh_4B_4$ *Phys. Rev. Lett.* **48** 950–3

[101] Prozorov R, Vannette M, Law S, Bud'ko S and Canfield P 2008 Coexistence of ferromagnetism and superconductivity in $ErRh_4B_4$ single crystals probed by dynamic magnetic susceptibility *Phys. Rev.* B **77** 100503

[102] Crespo V, Rodrigo J, Suderow H, Vieira S, Hinks D and Schuller I 2009 Evolution of the local superconducting density of states in $ErRh_4B_4$ close to the ferromagnetic transition *Phys. Rev. Lett.* **102** 237002

[103] Huang C Y, Olsen C E, Kozlowski G, Matsumoto H, Umezawa H, Mancini F, Maple M B, Hamaker H C, Torikachvili M S, Whitehead J P and Wang F E 1985 Anomalous surface impedance in reentrant ferromagnetic superconductors *J. Appl. Phys.* **57** 3104–6

[104] Hou M K, Huang C Y, Maple M B, Torikachvili M S and Hamaker H C 1986 Surface impedance of several magnetic superconductors *J. Magn. Magn. Mater.* **59** 247–9

[105] Mancini F and Noce C 1987 Electromagnetic properties of ferromagnetic superconducting films *Physica* B+C **145** 342–8

[106] Hamaker H C, Woolf L D, Mackay H B, Fisk Z and Maple M B 1979 Possible observation of the coexistence of superconductivity and long-range magnetic order in $NdRh_4B_4$ *Solid State Commun.* **31** 139–44

[107] Mackay H B, Woolf L D, Maple M B and Johnston D C 1980 ferromagnetism in the $ReRh_4B_4$ compounds *J. Low Temp. Phys.* **41** 639–51

[108] Cantor R H, Dahlberg E D, Goldman A M, Toth L E and Christner G L 1980 Critical magnetic fields of superconducting thin films of $ErRh_4B_4$ *Solid State Commun.* **34** 485–8

[109] Nagamatsu J, Nakagawa N, Muranaka T, Zenitani Y and Akimitsu J 2001 Superconductivity at 39 K in magnesium diboride *Nature* **410** 63–4

[110] Zaitsev A, Schneider R, Hott R, Schwarz T and Geerk J 2007 Effect of a dc magnetic field on the microwave losses in MgB_2 thin films *Phys. Rev.* B **75** 212505

[111] Hakim N, Parimi P V, Kusko C, Sridhar S, Canfield P C, Bud'ko S L and Finnemore D K 2001 Microwave properties of superconducting MgB_2 *Appl. Phys. Lett.* **78** 4160–2

[112] Bhide M K, Kadam R M, Sastry M D, Singh A, Sen S, Aswal D K, Gupta S K and Sahni V C 2001 Magnetic field

dependent microwave absorption studies on a MgB_2 superconductor *Supercond. Sci. Technol.* **14** 572–5
[113] Buzea C and Yamashita T 2001 Review of the superconducting properties of MgB_2 *Supercond. Sci. Technol.* **14** R115–46
[114] Cullity B D and Graham C D 2009 *Introduction to Magnetic Materials* (Hoboken, NJ: John Wiley)
[115] Shull C G, Strauser W A and Wollan E O 1951 Neutron diffraction by paramagnetic and antiferromagnetic substances *Phys. Rev.* **83** 333–45
[116] Golosovsky M, Monod P, Muduli P K and Budhani R C 2012 Low-field microwave absorption in epitaxial $La_{0.7}Sr_{0.3}MnO_3$ films that results from the angle-tuned ferromagnetic resonance in the multidomain state *Phys. Rev.* B **85** 184418
[117] Kip A F 1953 Microwave resonance absorption in gadolinium metal *Rev. Mod. Phys.* **25** 229–31
[118] Arrott A 1957 Criterion for ferromagnetism from observations of magnetic isotherms *Phys. Rev.* **108** 1394–6
[119] Saerbeck T, Pereiro J, Wampler J, Stanley J, Wingert J, Shpyrko O G and Schuller I K 2013 Ferromagnetism in partially oxidized CuCl *J. Magn. Magn. Mater.* **346** 161–5
[120] Dernier P D and Marezio M 1970 Crystal structure of the low-temperature antiferromagnetic phase of $V2O_3$ *Phys. Rev.* B **2** 3771–6
[121] Imada M, Fujimori A and Tokura Y 1998 Metal–insulator transitions *Rev. Mod. Phys.* **70** 1039–263
[122] Shin S, Tezuka Y, Kinoshita T, Kakizaki A, Ishii T, Ueda Y, Jang W, Takei H, Chiba Y and Ishigame M 1992 Observation of local magnetic moments in the Mott transition of V_2O_3 by means of 3s photoemission *Phys. Rev.* B **46** 9224–7
[123] Jacobs I and Lawrence P 1967 Metamagnetic phase transitions and hysteresis in $FeCl_2$ *Phys. Rev.* **164** 866–78
[124] Stryjewski E and Giordano N 1977 Metamagnetism *Adv. Phys.* **26** 487–650
[125] Birgeneau R J, Yelon W B, Cohen E and Makovsky J 1972 Magnetic properties of $FeCl_2$ in zero field: I. Excitations *Phys. Rev.* B **5** 2607–15
[126] Binek C and Kleemann W 1994 Domainlike antiferromagnetic correlations of paramagnetic $FeCl_2$: a field-induced Griffiths phase? *Phys. Rev. Lett.* **72** 1287–90
[127] Pöppl A, Kevan L, Kimura H and Schwartz R N 1992 Modulated microwave absorption at low magnetic fields in a $Tl_2Ba_2CaCu_2O_{8+x}$ single crystal *Phys. Rev.* B **46** 8559–64
[128] Srinivasu V V, Thomas B, Hegde M S and Bhat S V 1994 Line shapes of field-dependent nonresonant microwave and rf absorption in high-T_c superconductors *J. Appl. Phys.* **75** 4131–6
[129] Lee S J, Tsai C C, Cho H, Seo M, Eom T, Nam W, Lee Y P and Ketterson J B 2009 Hysteretic characteristics of low-field microwave absorption of a Co thin film *J. Appl. Phys.* **106** 063922
[130] Yuan T, Jiang H, Widom A, Vittoria C, Drehman A, Chrisey D and Horwitz J 1995 Correlation of static magnetization and microwave absorption measurements on superconducting films of $YBa_2Cu_3O_{7-x}$ *Physica* C **242** 197–204
[131] Bhat S V, Ganguly P, Ramakrishnan T V and Rao C N R 1987 Absorption of electromagnetic radiation by superconducting $YBa_2Cu_3O_7$: an oxygen-induced phenomenon *J. Phys. C: Solid State Phys.* **20** L559–63
[132] Meissner W and Ochsenfeld R 1933 Ein neuer Effekt bei Eintritt der Supraleitfähigkeit *Naturwissenschaften* **21** 787–8
[133] Shaposhnikova T, Vashakidze Y, Khasanov R and Talanov Y 1998 Peculiarities of the vortex dynamics in $YBa_2Cu_3O_x$ single crystals as revealed by irreversible microwave absorption *Physica* C **300** 239–49